Using the Maximum Entropy Production approach to integrate energy budget modeling in a hydrological model

Audrey Maheu[1], Islem Hajji[2], François Anctil[2], Daniel F. Nadeau[2], René Therrien[3]

[1]Département des sciences naturelles, Université du Québec en Outaouais, Ripon, J0V 1V0, Canada
5 [2]Département de génie civil et de génie des eaux, Université Laval, Québec, G1V 0A6, Canada
[3]Département de géologie et de génie géologique, Université Laval, Québec, G1V 0A6, Canada

Correspondence to: Audrey Maheu (audrey.maheu@uqo.ca)

Abstract. Total terrestrial evaporation is a key process to understand the hydrological impacts of climate change given that warmer surface temperatures translate into an increase in the atmospheric evaporative demand. To simulate this flux, many
10 hydrological models rely on the concept of potential evaporation (PET) although large differences have been observed in the response of PET models to climate change. The Maximum Entropy Production (MEP) model of land surface fluxes offers an alternative approach to simulate terrestrial evaporation in a simple way while fulfilling the physical constraint of energy budget closure and providing a distinct estimation of evaporation and transpiration. The objective of this work is to use the MEP model to integrate energy budget modeling within a hydrological model. We coupled the MEP model with
15 HydroGeoSphere, an integrated surface and subsurface hydrologic model. As a proof-of-concept, we performed one-dimensional soil column simulations at three sites of the AmeriFlux network. The coupled HGS-MEP model produced realistic simulations of soil water content (RMSE between 0.03 and 0.05 $m^3 \, m^{-3}$, NSE between 0.30 and 0.92) and terrestrial evaporation (RMSE between 0.31 and 0.71 mm day^{-1}, NSE between 0.65 and 0.88) under semiarid, Mediterranean and temperate climates. At the daily time scale, HGS-MEP outperformed the standalone HGS model where total terrestrial
20 evaporation is derived from potential evaporation which we computed using the Penman-Monteith equation, although both models had comparable performance at the half-hourly time scale. This research demonstrated the potential of the MEP model to improve the simulation of total terrestrial evaporation in hydrological models, including for hydrological projections under climate change.

1 Introduction

25 Driven by climate change, warmer surface temperatures are expected to increase the atmospheric evaporative demand (Breshears et al., 2013; Ficklin and Novick, 2017). As such, total terrestrial evaporation (herein after terrestrial evaporation), or "evapotranspiration", is a key process to assess the impacts of climate change on stream discharge. To simulate this flux, many hydrological models rely on the concept of potential evaporation (PET), which is defined as the maximum evaporation that can occur under ambient meteorological conditions with an unlimited water supply. Two types of PET models are
30 generally used in hydrological models: temperature-based models where PET is estimated via air temperature (Thornthwaite, 1948; Hamon, 1963) and physically based models where PET estimation is based on components of the surface energy budget (Monteith, 1965; Priestley and Taylor, 1972). Various studies have compared PET models to assess their suitable range of application (Xu and Singh, 2001). While the performance of PET models varies across regions, the choice of a PET model appears to have minimal influence on stream discharge simulation under contemporary climate conditions
35 (Andréassian et al., 2004; Oudin et al., 2005; Isabelle et al., 2018). However, when future climate projections are incorporated in PET models, the predicted PET varies significantly from model to model (McKenney and Rosenberg, 1993; Kingston et al., 2009; Donohue et al., 2010; Lofgren et al., 2011; McAfee, 2013; Hosseinzadehtalaei et al., 2016). These differences often translate into large uncertainty in stream discharge projections (Kay and Davies, 2008; Bae et al., 2011; Milly and Dunne, 2011; Prudhomme and Williamson, 2013; Seiller and Anctil, 2016), although some studies have
40 demonstrated opposite results with a relatively low sensitivity of discharge projection to PET model selection (Thompson et al., 2014; Koedyk and Kingston, 2016).

Among PET models, those that are temperature-based tend to mainly reflect changes in mean air temperature, even though temperature is not necessarily the strongest control on PET (Donohue et al., 2010; Shaw and Riha, 2011). For example, the oversensitivity of temperature-based models to surface warming has been linked to an exaggerated assessment of drought severity under climate change (Hoerling et al., 2012). As a result, recent studies have recommended the use of physically based PET models, such as the Penman model, to simulate terrestrial evaporation in climate change assessments (Hobbins et al., 2008; Sheffield et al., 2012; McAfee, 2013). However, additional data inputs (e.g., radiation, humidity and wind speed) are required to implement such models and, as opposed to the high confidence put in temperature estimates from global climate models (McMahon et al., 2015), these variables usually suffer from a lower reliability. For example, large differences persist between observations, reanalysis products and global climate model projections of wind speed (McVicar et al., 2008; Pryor et al., 2009). Overall, a dilemma emerges for the simulation of PET under climate change, which involves choosing between a reliable physically based model with greater input data uncertainty versus an overly simplified temperature-based model with reliable input data (Ekström et al., 2007; Kay and Davies, 2008; Kingston et al., 2009).

Given these current limitations with PET models, alternative approaches are needed for the simulation of terrestrial evaporation in climate change assessments. Energy budget modeling offers a physically based approach to simulate terrestrial evaporation (along with other components of the surface energy budget), with the added benefit of conservation of energy that ensures a balance between incoming and outgoing energy. Land surface models provide a means to simulate both water and energy budgets and they have been used for hydrological modeling, either by i) coupling hydrological and land surface models (Pietroniro et al., 2001; Maxwell and Miller, 2005; Kunstmann et al., 2008; Zabel and Mauser, 2013) or by ii) coupling a land surface model to a routing scheme (Gaborit et al., 2017). In land surface models, terrestrial evaporation is generally estimated with a bulk aerodynamic approach (Noilhan and Planton, 1989) that relies on semi-empirical equations and requires information on vertical gradients of air temperature and humidity that can introduce substantial errors. The use of land surface models can yield small gains in hydrological modeling performance (Livneh et al., 2011; Shi et al., 2014), but they remain computationally heavy.

Optimality principles, which are derived from the idea that nature organizes itself to ensure optimal functioning, provide an alternative avenue to model terrestrial evaporation. Maximum entropy production (MEP) is one of the optimality principles put forward and, although it has yet to become an established principle, it offers a promising method to improve hydrological modeling (Ehret et al., 2014; Westhoff and Zehe, 2013). The MEP principle has been applied in two ways in hydrology. In the first approach, MEP is defined as a physical principle, which hypothesizes that an open thermodynamic system far from equilibrium can achieve a steady state at which, through self-organization, entropy is produced at the maximum possible rate. Such a dynamic equilibrium can be achieved because, as demonstrated by Paltridge (1975), a gradient drives a flux that in turn, depletes the initial gradient and further reinforces it. Using this approach, MEP has been used to constrain parameters of hydrological models (Kleidon and Schymanski, 2008; Porada et al., 2011; Westhoff and Zehe, 2013). In the second approach, MEP is defined as a statistical principle and constitutes the most probable state of an open system (Dewar, 2005; 2009). Using the MaxEnt statistical inference algorithm (Jaynes, 1957), the state of MEP can be predicted by maximizing Shannon information entropy while considering constraints imposed by the available information. Wang and Bras (2009, 2011) used this approach to develop the MEP model of land surface fluxes, which is the topic of the present article.

The MEP model of land surface fluxes (Wang and Bras, 2009, 2011) offers a simple approach for energy budget modeling that ensures the closure of the surface energy balance. In the MEP model developed by Wang and Bras, only three input variables, net radiation, surface temperature and surface specific humidity, are required to model surface heat fluxes, with a different definition of the surface when assessing evaporation (surface = soil) and transpiration (surface = leaf). As it will be presented below, in practice, the following six input variables are needed to operate MEP continuously under all climate conditions: net radiation, soil surface temperature and specific humidity, leaf surface temperature and specific humidity and a vegetation index. Overall, the MEP model eliminates the need for wind speed and surface roughness data (i.e. input data to the Penman model) as well as eliminating the need for data on vertical gradients (i.e. temperature and humidity, input data to the bulk aerodynamic model often implemented in land surface models). Moreover, the predicted surface heat fluxes are constrained by the available energy (i.e. net radiation), which avoids the issue of oversensitivity to temperature and suggests

that this approach should be robust for climate change assessments. Recent studies also reported improved performance of the MEP approach for the simulation of terrestrial evaporation when compared against the Penman-Monteith model (Hajji et al., 2018) or a modified Penman-Monteith approach driven by remote sensing and reanalysis data (Xu et al., 2019). The MEP model also had a performance comparable to a complex land surface model (Canadian Land Surface Scheme, CLASS) at snow-free sites at low latitudes (Alves et al., 2019). Overall, the MEP model offers an attractive approach to improve the simulation of terrestrial evaporation in hydrological modeling and to increase the robustness of streamflow projections under climate change. The objective of this study is thus to couple the MEP model of land surface fluxes with a hydrological model and perform proof-of-concept simulations at AmeriFlux sites spanning a range of climatic and vegetation conditions.

2 Study area

We selected three sites of the AmeriFlux network (Baldocchi et al., 2001) where the eddy covariance method is used to measure vertical water and energy fluxes (Table 1, Figure 1). We selected sites using the following criteria: i) measurements of volumetric soil water content available at different depths and for an extended period; ii) absence of snow cover and iii) diversity in climates (semiarid, Mediterranean, temperate) and types of vegetation (grassland, woody savanna, deciduous broadleaf forest).

Table 1. Description of study sites

	US-Wkg	US-Ton	US-WBW
climate	semiarid	Mediterranean	temperate
Koppen climate class	Bsk: steppe, warm winter	Csa: Mediterranean, mild with dry, hot summer	Cfa: humid subtropical, mild with no dry season, hot summer
IGPB vegetation class	grassland	woody savanna	deciduous broadleaf forest
mean annual precipitation (mm)	407	559	1372
mean annual temperature (°C)	15.6	15.8	13.7
data source	Scott (2016)	Baldocchi (2016)	Meyers (2016)
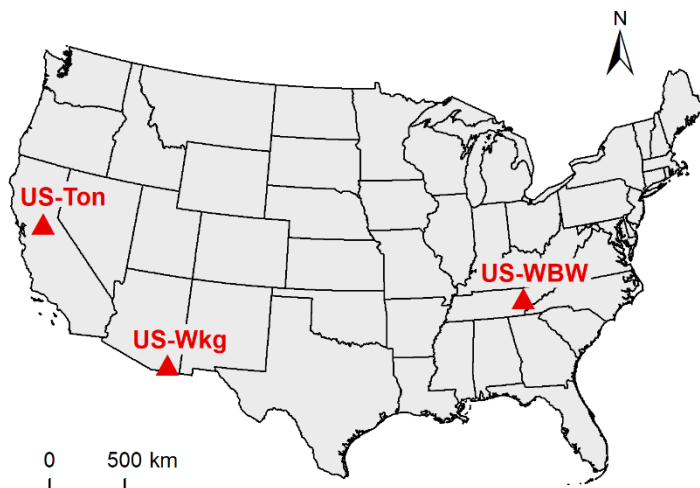
Figure 1. Location of study sites across the conterminous United States

The first site, US-Wkg, is characterized by a semiarid climate where 60% of precipitation is concentrated in July, August, and September. In 2006, a sharp transition occurred in the vegetation and the native grassland species (assemblage of grama grasses, genus *Bouteloua*) have been supplanted by Lehman lovegrass (*Eragrostis lehmanniana*), an exotic species spreading

throughout southwestern United States (Moran et al., 2009; Scott et al., 2010). The second site, US-Ton, is characterized by a Mediterranean climate with dry summers and most precipitation occurring from October to May. The woody savanna is made up of two layers of vegetation, each reaching peak activity at different times of the year (Baldocchi et al., 2004). Trees, mainly blue oaks (*Quercus douglasii*), are dormant during winter months, reach peak activity in the spring and then carefully regulate their water use during the dry summer period. In contrast, the understory vegetation composed of grasses and forbs is mainly active during the rainy winter period when water is plentiful. Finally, the US-WBW site is characterized by a temperate climate with precipitation relatively evenly distributed throughout the year. The mixed deciduous forest is dominated by oak and hickory and vegetation is active from the spring to early autumn (April to October), with peak activity during the summer (Wilson and Baldocchi, 2000).

3 Methodology

3.1 Maximum entropy production (MEP) model

The MEP model of land surface fluxes uses the optimality principle of maximum entropy production (Dewar, 2005) as an inference tool for nonequilibrium thermodynamic systems. In the MEP model, entropy refers to Shannon entropy, the expected value of information (Shannon, 1948), which is not related to thermodynamic entropy expressed as the ratio of flux to temperature. Indeed, the MEP model is derived from the principle of maximum entropy (MaxEnt) developed by Jaynes (1957) as a general inference tool to assign probability distributions in statistical mechanics. Wang and Bras (2009) used this statistical approach to develop the MEP model of land surface fluxes. Within the MEP model, land surface fluxes are each expressed in terms of a dissipation or entropy function and, under the constraint of conservation of energy, a unique extremum solution is found.

Dissipation functions have been postulated for land surface fluxes over a dry soil (Wang and Bras, 2009) and over wet soil and vegetation surfaces (Wang and Bras, 2011). For non-vegetated surfaces, bare soil evaporation (E_s) is estimated by solving equations 1 and 2 with the constraint of energy conservation at the surface ($R_n = G + E_s + H$) (Wang and Bras, 2011):

$$E_s = B(\sigma)H \tag{1}$$

$$G = \frac{B(\sigma)}{\sigma}\frac{I_s}{I_0}H|H|^{-\frac{1}{6}} \tag{2}$$

where R_n, E_s, H and G are the net radiation, latent, sensible and ground heat fluxes at the soil surface (W m^{-2}; positive values indicate a heat flux away from surface), $B(\sigma)$ is the inverse of the Bowen ratio (see equation 7), σ is a dimensionless parameter (see equation 8). I_s is the soil thermal inertia (J m^{-2} K^{-1} s$^{-1/2}$), calculated with the empirically derived equation from Huang and Wang (2016):

$$I_s = \sqrt{I_{ds}^2 + \theta I_w^2} \tag{3}$$

where I_{ds} is the dry soil thermal inertia (J m^{-2} K^{-1} s$^{-1/2}$), θ is the volumetric soil moisture (m^3 m^{-3}) and I_w is the thermal inertia of liquid water (1557 J m^{-2} K^{-1} s$^{-1/2}$). I_0 is the "apparent thermal inertia of air" (J m^{-2} K^{-1} s$^{-1/2}$) and was calculated as:

$$I_0 = \rho_a c_p \sqrt{C_1 kz}\left(C_2\frac{kzg}{\rho_a c_p T_0}\right)^{1/6} \tag{4}$$

where ρ_a is the air density (1.22 kg m^{-3}), c_p is specific heat of air under constant pressure (1004 J kg^{-1} K^{-1}), C_1 and C_2 are two constants in the empirical functions representing the effects of stability on the mean profiles of wind speed and temperature within the surface layer (Wang and Bras, 2009), k is the von Kármán constant (0.4), z is the height above ground based on vegetation conditions (m), g is the gravitational acceleration (9.81 m s^{-2}) and T_0 is a reference temperature (300 K).

For vegetated surfaces, the MEP model of transpiration considers the energy balance at the vegetation surface. As such, the term G corresponds to the canopy heat flux (not to be confused with the ground heat flux G in the MEP model for non-vegetated surfaces, equations 1-2) and is considered negligible compared to the sensible and latent heat fluxes (Wang and Bras, 2011). Accordingly, the energy balance is simplified and transpiration (E_t) is estimated by solving equations 5 and 6 under the constraint of energy conservation at the surface ($R_n = E_t + H$):

$$E_t = \frac{R_n}{1+B^{-1}(\sigma)} \tag{5}$$

$$H = \frac{R_n}{1+B(\sigma)} \tag{6}$$

The same definition of $B(\sigma)$ and σ applies for non-vegetated (equations 1-2) and vegetated (equations 5-6) surfaces and the Bowen reciprocal ratio is calculated as:

$$B(\sigma) = 6\left(\sqrt{1 + \frac{11}{36}\sigma} - 1\right) \tag{7}$$

where σ corresponds to a dimensionless parameter that characterizes the phase change at the evaporating or transpiring surface:

$$\sigma = \frac{\sqrt{\alpha}\lambda^2}{c_p R_v} \frac{q_s}{T_s^2} \tag{8}$$

where α is the ratio of the eddy diffusivities for water vapor and heat (assumed to be unity, (Wang et al., 2014), λ is the latent heat of vaporization of liquid water (J kg^{-1}), C_p is the specific heat of air under constant pressure (J kg^{-1} K^{-1}), R_v is the gas constant of water vapor (461 J kg^{-1} K^{-1}), q_s is the surface specific humidity (kg kg^{-1}), and T_s is the surface temperature (K).

In the MEP model of evaporation (MEP-E$_s$, equations 1-2), the surface specific humidity (q_s) corresponds to the specific humidity at the soil surface (q_{ss}) and the surface temperature (T_s) corresponds to skin temperature at the soil surface (T_{ss}). Equation 8 can be modified accordingly:

$$\sigma = \frac{\lambda^2}{c_p R_v} \frac{q_{ss}}{T_{ss}^2} \tag{9}$$

The specific humidity at the soil surface can be computed as (Huang and Wang, 2016):

$$q_{ss} = \left(\frac{\theta}{\theta_s}\right)^\beta q_{sat} \tag{10}$$

where q_{sat} is the specific humidity at saturation (kg kg^{-1}) at T_{ss} which is calculated using the Clausius-Clapeyron equation, θ is the soil water content (m^3 m^{-3}), θ_s is the soil porosity (m^3 m^{-3}) and β is an empirical parameter that was set to $\beta = 2$ based on Huang and Wang (2016).

In the MEP model of transpiration (MEP-E$_t$, equations 5-6), the surface specific humidity (q_s) corresponds to the specific humidity at the leaf surface (q_{ls}) and the surface temperature (T_s) corresponds to the leaf temperature (T_{ls}). A water stress factor (η_s) that varies between 0 and 1 is added to the original formulation of equation 8 presented by Wang and Bras (2011) to describe the reduction in plant transpiration under soil water stress (Hajji et al., 2018). For MEP-E$_t$, equation 8 thus translates into:

$$\sigma = \eta_s \frac{\lambda^2}{c_p R_v} \frac{q_{ls}}{T_{ls}^2} \tag{11}$$

Various parameterizations of η_s exist in the literature based on soil water potential (Verhoef and Egea, 2014; Ferguson et al., 2016), volumetric soil water content (Feddes et al., 1978; Porporato et al., 2001) or leaf water potential (Tuzet et al., 2003).

We used the Wang and Leuning (1998) parameterization of η_s based on soil water content that Hajji et al. (2018) successfully used to apply the MEP model of transpiration under water-limiting conditions:

$$\eta_s = \min\left[1, \frac{10\,(\theta_{root} - \theta_{wp})}{3\,(\theta_{fc} - \theta_{wp})}\right] \qquad (12)$$

where θ_{root} is the weighted average soil water content over the root zone, with weights set according to the vertical root distribution (m³ m⁻³), θ_{wp} is the soil water content at wilting point (m³ m⁻³) and θ_{fc} is the soil water content at field capacity (m³ m⁻³).

The MEP models have been formulated for the two limiting cases of bare soil evaporation and transpiration from a fully vegetated surface. In order to continuously simulate terrestrial evaporation, Hajji et al. (2018) proposed a method to combine the MEP models of evaporation and transpiration using a vegetation index (f_{veg}) that corresponds to the fraction of the soil covered by vegetation. Assuming that evaporation from intercepted rainfall is negligible, as is the case in this study, the MEP model of terrestrial evaporation (MEP-E) is then defined as:

$$E = \left(1 - f_{veg}\right)E_s + f_{veg}E_t \qquad (13)$$

The vegetation index (f_{veg}) can be derived from the Normalized Difference Vegetation Index (NDVI) (Gutman and Ignatov, 1998):

$$f_{veg} = \frac{NDVI_t - NDVI_{\min}}{NDVI_{\max} - NDVI_{\min}} \qquad (14)$$

where $NDVI_t$ is the NDVI on day t, $NDVI_{\min}$ is the NDVI signal from bare soil and $NDVI_{\max}$ is the NDVI signal from a full vegetation cover.

3.2 Hydrological model

HydroGeoSphere (HGS) is an integrated surface and subsurface hydrologic model that has been used to simulate soil water content at various AmeriFlux sites (Maheu et al., 2018) as well as in a forested headwater catchment (Koch et al., 2016). Maxwell et al. (2014) performed a formal verification of seven integrated surface and subsurface models and HGS showed good agreement with other models when simulating soil moisture in an idealized test case. HGS is a control-volume finite-element model that simultaneously solves the 2-D diffusion-wave approximation of the Saint-Venant equations and the 3-D form of the Richards equation (Aquanty, 2013). The surface and subsurface are coupled via a first-order exchange coefficient. The commonly used van Genuchten (1980) model is incorporated in HGS to describe the water retention curve. HGS has an adaptive time-stepping procedure where the time step length is controlled by the maximum change allowed in a state variable during any time step. In the present study, we allowed for a maximum change of 0.05 in soil saturation. In the current version of HGS, transpiration and evaporation are simulated as a function of potential evaporation (Kristensen and Jensen, 1975):

$$E_t(z) = f_1(LAI)\,f_2(\theta)\left(E_p - E_c\right)r(z) \qquad (15)$$

where $E_t(z)$ is the transpiration rate (m s⁻¹) at depth z, E_p is the potential evaporation rate (m s⁻¹), E_c is the wet canopy evaporation rate (m s⁻¹). $f_1(LAI)$ is a function of the leaf area index (LAI) representing changes in vegetation over time (dimensionless):

$$f_1(LAI) = max\{0, min[1, C_2 + C_1 LAI]\} \qquad (16)$$

where C_1 and C_2 are dimensionless fitting parameters. $f_2(\theta)$ is a function describing the water stress on vegetation (dimensionless) which is equivalent to η_s (equation 12). $r(z)$ is the root distribution function which follows a cubic decay distribution between the surface and the maximum root depth. Soil evaporation is described as:

$$E_s(z) = \alpha^*\left[1 - f_1(LAI)\right]\left(E_p - E_c\right)e(z) \qquad (17)$$

where $E_s(z)$ is the soil evaporation rate (m s^{-1}) at depth z, $e(z)$ is the evaporation depth function which follows a cubic decay distribution between the surface and the maximum evaporation depth. α^* is a soil wetness factor (dimensionless):

$$\alpha^* = \begin{cases} \frac{\theta-\theta_{e2}}{\theta_{e1}-\theta_{e2}} & \text{for } \theta_{e2} \leq \theta \leq \theta_{e1} \\ 1 & \text{for } \theta > \theta_{e1} \\ 0 & \text{for } \theta < \theta_{e2} \end{cases} \qquad (18)$$

where θ_{e1} is the soil water content above which full evaporation occurs and θ_{e2} is the soil water content below which
5   evaporation is zero.

3.3 Coupling the HGS and MEP-E models

In the HGS model, the following modified form of Richards equation is used to describe the temporal evolution of soil moisture:

$$-\nabla \cdot \mathbf{q} + \sum \Gamma_{ex} \pm Q = \frac{\partial}{\partial t}(\theta_s S_w) \qquad (19)$$

10   where $\mathbf{q}$ is the specific volumetric (Darcy) flux (m^3 s^{-1}), Γ_{ex} is the source/sink term for exchange fluxes with other domains (i.e. surface) (m^3 s^{-1}), Q is the source/sink term for the porous medium such as pumping or injection (m^3 s^{-1}) and S_w is the subsurface water saturation (m^3 m^{-3}). The MEP-E$_s$ model requires soil moisture information to compute three parameters: the soil thermal inertia (I_s, equation 3) and the surface specific humidity of the soil (q_{ss}, equation 9) and leaf (q_{ls}, equation 11) surfaces. At the beginning of a given time step, HGS supplies the soil moisture information from the previous time step to the
15   MEP-E model which then computes the evaporation and transpiration rates (Figure 2). The transpiration and evaporation rates computed with the MEP-E model are then transferred to HGS and taken as sinks for the porous medium (Γ_{ex} in equation 19). HGS removes water from the soil reservoir based on the root and evaporation depth profiles, which both follow a cubic decay distribution between the surface and the maximum root or evaporation depth. At the end of the given time step, HGS calculates the saturation throughout the soil column. Given that the MEP-E$_s$ model was not very sensitive to changes in soil
20   thermal inertia, this parameter was set as a constant equal to the dry soil thermal inertia (as detailed in the next section) and was not involved in the coupling procedure.
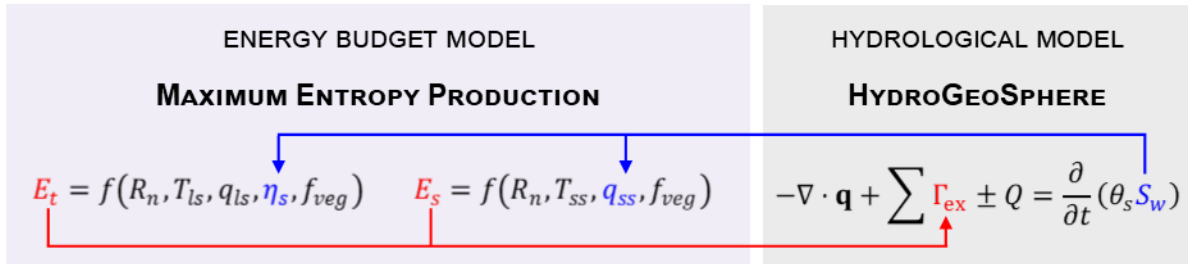
Figure 2. Coupling of the HydroGeoSphere (HGS) hydrological model and the Maximum Entropy Production (MEP) model of
25   **land surface fluxes. HGS supplies the MEP model with soil water saturations (S_w, in blue) which are used by the MEP model to compute the transpiration (E_t) and evaporation (E_s) rates. These rates are then passed on to HGS to compute the sink terms with the surface (Γ_{ex}, in red) and HGS removes water from the soil reservoir based on the root and evaporation depth profiles.**

3.4 Model implementation

3.4.1 HGS-MEP

30   The coupled HGS-MEP model was not calibrated in the present study. The soil and vegetation properties were therefore not obtained from calibration but were rather defined from pedo-transfer functions, observations at AmeriFlux sites or values taken from the literature. We derived soil hydraulic characteristics (Table 2) using soil texture information as an input to the

Rosetta model implemented in Hydrus (Šimůnek et al., 2013) to derive the soil hydraulic characteristics. Soil texture information was either taken from the AmeriFlux database (US-Ton) or from the literature (US-Wkg in Nearing et al., 2005 and US-WBW in Miller et al., 2007). At US-Wkg and US-Ton, the observed minimum soil water content was smaller than residual saturation computed by the Rosetta model and, as such, we set the residual saturation in HGS to the observed minimum soil water content. At each site, we defined soil porosity as the observed maximum soil water content closest to the surface and we used the water retention curve to compute the volumetric water content corresponding to the wilting point (–1.5 MPa) and field capacity (–0.033 MPa). We defined the maximum root depth using site-specific information at US-Ton (Ichii et al., 2009) and US-WBW (Wilson et al., 2001). Given that similar information was unavailable at US-Wkg, we set the maximum root depth based on the root depth reported for Lehman lovegrass in the literature (Gibbens and Lenz, 2001), the main grass species at the site. Given only little information is available on soil and root properties, parameter allocation for these properties is often an important source of uncertainty in hydrological models. However, previous modeling work at the study sites has shown soil moisture modeling to be relatively robust to variations in saturated hydraulic conductivity and vertical root distribution (Maheu et al., 2018).

Table 2. Soil and vegetation properties at each study site

	US-Wkg	US-Ton	US-WBW
% sand – silt – clay [a]	55 – 20 – 25	48 – 42 – 10	28 – 60 – 12
saturated hydraulic conductivity (x10^{-6} m s^{-1})	2.813	2.929	3.615
residual saturation (m^3 m^{-3})	0.01	0.02	0.05
wilting point (m^3 m^{-3})	0.05	0.07	0.07
field capacity (m^3 m^{-3})	0.21	0.29	0.26
porosity (m^3 m^{-3})	0.44	0.56	0.38
root depth (m)	1.2	0.7	0.6

[a] US-Wkg: Nearing et al. (2005); US-Ton: BADM from the AmeriFlux database; US-WBW: Miller et al. (2007)

Table 3 provides a summary of the implementation of the MEP model of terrestrial evaporation in HGS. In the MEP model of evaporation, skin temperature measurements would ideally be used to set the soil surface temperature (T_{ss}) but, since those measurements were not available, we instead used soil temperature measurements nearest to the surface, that is at a depth of 5 cm at US-Wkg, 2 cm at US-Ton and 2 cm at US-WBW. The height above ground (z in equation 4) was set to the flux tower height, which was 6.4 m at US-Wkg, 23 m at US-Ton and 36.9 m at US-WBW. At US-Wkg, the dry soil thermal inertia (I_{ds} in equation 3) was computed according to Wang et al. (2010) as the regression coefficient between diurnal variations in the ground heat flux and surface temperature (830 J m^{-2} K^{-1} s$^{-1/2}$). Because these data were unavailable at US-Ton and US-WBW and given that the model showed little sensitivity to the soil thermal inertia, the dry soil thermal inertia was set equal to 800 J m^{-2} K^{-1} s$^{-1/2}$ for these two sites. In the MEP model of transpiration, the leaf surface temperature was assumed equal to the air temperature measured above the canopy. Since no measurements of the leaf surface specific humidity were available, we used the specific humidity of the air as a proxy and calculated it from air temperature and relative humidity measurements using the Clausius-Clapeyron equation. To combine the MEP models of evaporation and transpiration (equation 13), we computed the vegetation index (equation 14) using the AVHRR 7-day composite NDVI (https://lta.cr.usgs.gov/NDVI). NDVI time series are notoriously noisy because of varying atmospheric conditions and sensor viewing angles (Hird and McDermid, 2009) and we therefore smoothed the time series by applying a 60-day moving average. Based on Montandon and Small (2008), the NDVI signal for bare soil ($NDVI_0$) was set to 0.2 and the NDVI signal for full vegetation cover varied according to the land cover, with $NDVI_\infty = 0.61$ for grassland, $NDVI_\infty = 0.69$ for woody savanna, and $NDVI_\infty = 0.85$ for deciduous broadleaf forest.

Table 3. Implementation of the MEP model of total terrestrial evaporation in this study

Model	Variable	Definition	Implementation
MEP-E$_s$	R_n	net radiation	net radiation measurements
	T_{ss}	surface temperature	soil temperature measurements nearest to the surface
	q_{ss}	surface specific humidity	equation 10; computed from soil water content (supplied by HGS), porosity (Table 2) and surface temperature measurements
	I_s	soil thermal inertia	set as a constant in this study
MEP-E$_t$	R_n	net radiation	net radiation measurements
	T_{ls}	surface temperature	air temperature measurements at top of the tower
	q_{ls}	surface specific humidity	computed from air temperature and relative humidity measurements at the top of the tower
	η_s	water stress factor	equation 12; computed from the soil water content (supplied by HGS) and the soil water content at wilting point and field capacity (Table 2)
MEP-E	f_{veg}	vegetation index	equation 14; computed from NDVI data

3.4.2 HGS with Penman-Monteith (HGS-PM)

We compared HGS-MEP to simulations of terrestrial evaporation and soil water content performed with the standalone HGS model, in which the Kristensen and Jensen (1975) model is implemented, as described in section 3.2. We used the same soil and root properties defined for the HGS-MEP simulations (Table 2) and the only difference lied in the terrestrial evaporation model. In HGS, transpiration and evaporation are set to occur simultaneously. However, this approach led to a large overestimation of terrestrial evaporation. In the present study, we modified the implementation of the model and evaporation took place only when $f_1(LAI) = 0$. As for the HGS-MEP model implementation, interception was not considered and E_c was set to zero. The maximum and minimum evaporation limiting saturation (equation 18) were set to 0.1 ($\theta_{e1} = 0.1\theta_s$) and 0.5 ($\theta_{e2} = 0.5\theta_s$) (Verbist et al., 2012). Potential evaporation (E_p), that is terrestrial evaporation from a saturated land surface, was computed with the Penman-Monteith equation, a physically based model where, similar to the MEP model, the predicted terrestrial evaporation is constrained by available energy at the surface:

$$E_p = \frac{1}{\lambda} \frac{\Delta(R_n - G) + \frac{\rho_a c_p (e_s - e_a)}{r_a}}{\Delta + \gamma\left(1 + \frac{r_s}{r_a}\right)} \qquad (20)$$

where Δ is the slope of the saturation vapor pressure curve (kPa K^{-1}), e_s is the saturation vapor pressure (kPa), e_a is the actual vapor pressure (kPa), γ is the psychrometric constant (kPa K^{-1}), r_s is the surface resistance (m s^{-1}) and r_a is the aerodynamic resistance (m s^{-1}). When $f_1(LAI) > 0$, the surface resistance (r_s) was set according to the vegetation lookup table in the Noah land surface model (US-Wkg = 40 s m^{-1}, US-Ton = 70 s m^{-1}, US-WBW = 100 s m^{-1} in Kumar et al., 2011) and the canopy aerodynamic resistance (r_{ac}) was computed as (Thom, 1975):

$$r_{ac} = \frac{1}{\kappa^2 u}\left[\ln\left(\frac{z - d_0}{z_{0m}}\right)\ln\left(\frac{z - d_0}{z_{0v}}\right)\right] \qquad (21)$$

where u is the wind speed (m s^{-1}), z is the wind speed measurement height (m), d_0 is the zero-plane displacement height (m), z_{0m} is the roughness height for momentum transfer (m) and z_{0v} is the roughness height for water vapor transfer (m). Equation 21 was derived for neutral atmospheric conditions but has also been successfully used to model terrestrial evaporation over a wide range of conditions (Ershadi et al., 2014). Roughness heights were estimated as a fraction of the vegetation height, h (m) (Brutsaert, 1982):

$$d_0 = 0.66h \qquad (22)$$

$$z_{0m} = 0.1h \tag{23}$$

$$z_{0v} = 0.1z_{0m} \tag{24}$$

When $f_1(LAI) = 0$, the surface resistance (r_s) was set to 999 s m^{-1}, the value associated with a barren/sparsely vegetated land cover in the Noah lookup table (Kumar et al., 2011), and the substrate aerodynamic resistance (r_{as}) was computed as (Shuttleworth and Wallace, 1985):

$$r_{as} = \frac{1}{\kappa^2 u}\left[\ln\left(\frac{z}{z_0'}\right)\ln\left(\frac{d_0+z_{0m}}{z_0'}\right)\right] \tag{25}$$

where z_0' is the roughness length of the soil (m) which was set to 0.01 m (Shuttleworth and Wallace, 1985).

The $f_1(LAI)$ function used to describe temporal changes in vegetation (equation 16) was computed by rescaling the vegetation index f_{veg}, an input to the HGS-MEP model, between 0 and 1.

3.5 Model setup

As a proof-of-concept, we set up the coupled HGS-MEP and HGS-PM models to perform one-dimensional soil column simulations to evaluate the capability of both models to simulate water fluxes (terrestrial evaporation) and storage (soil moisture). We represented the soil column with a fine (1 cm) vertical resolution and set the soil column depth to either 1 or 1.5 m in order to capture the entire root zone at each site. We assigned uniform soil properties throughout the soil column since there was no available data to describe the vertical distribution of soil material with depth. Simulations spanned five years at US-Wkg and US-Ton and 2.5 years at US-WBW given data were not available for a longer period. We used soil water content measurement available at different depths to set initial subsurface conditions and we used linear interpolation to assign initial conditions at depths without measurements. As for initial surface water conditions, we assumed an initial surface water depth of zero given the soil was not fully saturated. For boundary conditions, we supplied the model with gap-filled (REddyProc, Reichstein et al., 2005) measurements of precipitation, net radiation, air temperature, relative humidity and soil temperature at a 30-minute time step. At the surface, we applied a critical depth boundary condition that allows water to leave the model domain via overland flow. At the bottom of the soil column, we applied a free drainage boundary condition.

3.6 Model performance

We evaluated the performance of models using a series of metrics comparing observed and simulated values of terrestrial evaporation and soil water content at the three sites. First, we computed the root mean square error (RMSE) to assess the mean difference between observed and simulated values. Second, we computed the Nash-Sutcliffe efficiency (NSE), where a value of one indicates a perfect agreement between the model and observations and a negative value indicates that average value of observations offers a better predictor than the model. The RMSE and NSE are not independent metrics of performance given that the NSE is a standardized measure of the mean square error. Still, we chose to report the two commonly used metrics as they provide an assessment of performance in absolute (RMSE) and relative (NSE) terms. Third, we computed the normalized benchmark efficiency (BE), which is analog to the NSE, but rather compares the model output to a simple benchmark model, in this case, the interannual mean value for every calendar day (Schaefli and Gupta, 2007). Fourth, we computed the coefficient of determination (R^2) that describes the proportion of the total variance in observations explained by the model. Finally, we computed the percent bias (PBIAS) to assess the average tendency of simulated values to be larger (positive bias) or smaller (negative bias) than observations. Equations of performance metrics are listed in Table S1.

We calculated performance metrics at half-hourly and daily time scales for terrestrial evaporation and at a daily time scale for soil water content. When assessing the ability of the models to simulate terrestrial evaporation, we first calculated performance metrics on the entire time series and second, assessed how well the models performed under water-limited conditions. To do so, we computed the monthly aridity index, that is the ratio between precipitation and PET, where PET was calculated with the Penman-Monteith equation (eq. 20). Using monthly values of the aridity index, we then calculated

performance metrics for dry periods (P/PET < 0.4 at US-Wkg and P/PET < 1 at US-Ton and US-WBW) and wet periods (P/PET ≥ 0.4 at US-Wkg and P/PET ≥ 1 at US-Ton and US-WBW). As US-Wkg is located in a semi-arid climate, we used a different threshold (0.4) to define water-limited conditions as the monthly aridity index remained below one for the entire study period.

5 **4 Results**

4.1 Model performance under a semiarid climate (US-Wkg)

During the study period (2010–2014), the mean annual precipitation at US-Wkg varied between 264 and 415 mm, with 2013 and 2014 being the driest and wettest years, respectively (Figure 3a). Between January and June, pre-monsoon precipitation was relatively low (≤ 35 mm), with the exception of 2010, which saw 110 mm of rain in the first six months of the year.
10 Precipitation was concentrated during the monsoon periods and, with the exception of 2010, nearly 80% occurred between July and September. Figure 3b shows that the HGS-MEP model provided a realistic simulation of soil moisture at 15 cm depth (RMSE = 0.04 m^3 m^{-3}; NSE = 0.30; Table 4) and was able to capture the sharp rise in soil moisture at the start of the monsoon period in July – note that soil moisture observations were missing for the 2010/217 to 2011/365 period. Overall, soil moisture at 15 cm depth was generally overestimated (PBIAS = 19%; Table 4) with HGS-MEP, particularly the lower values
15 outside the monsoon period. For example, the observed annual minimum in soil water content was 0.06 m^3 m^{-3} between 2012 and 2014, while modeled soil moisture did not fall below 0.12 m^3 m^{-3}. A similar overestimation was also observed for the upper ($z = 5$ cm) and lower ($z = 30$ cm) soil layers (Figure S1).

Figure 3c shows that the HGS-MEP model also performed well in simulating the daily mean terrestrial evaporation (RMSE = 0.31 mm day^{-1}; NSE = 0.88; Table 4). The HGS-MEP model reproduced the seasonal pattern in terrestrial evaporation and
20 captured the sharp increase associated with the increased soil water availability from July to September. Peak terrestrial evaporation was slightly underestimated by HGS-MEP (PBIAS = –10%; Table 4). For example, the observed annual maximum ranged between 4.8 and 5.8 mm day^{-1}, while the modeled annual maximum did not exceed 4.0 mm day^{-1}. The HGS-MEP model was also able to simulate the increase in terrestrial evaporation following precipitation events outside the monsoon months. However, the pre-monsoon months were particularly wet in 2010 and terrestrial evaporation simulated by
25 HGS-MEP was underestimated with a modeled average of 0.5 mm day^{-1} between January and May compared to an observed average of 0.9 mm day^{-1}. At US-Wkg, terrestrial evaporation was dominated by evaporation, particularly during the dry season during which it represented 69% of the terrestrial evaporation simulated by HGS-MEP (Figure 4a). During the monsoon period when vegetation activity is concentrated (July to October), evaporation decreased in importance and, on average, accounted for 60% of the total terrestrial evaporation simulated by HGS-MEP, while transpiration represented 40%
30 of total terrestrial evaporation. These proportions varied from year to year. For example, 2014 was the wettest year during the study period and modeled transpiration represented 46% of total terrestrial evaporation during the monsoon period. In contrast, modeled transpiration represented 28% of total terrestrial evaporation during the monsoon period in 2012, although terrestrial evaporation was overall underestimated by the HGS-MEP model that year. Overall, the HGS-MEP model outperformed the HGS-PM model for the simulation of daily terrestrial evaporation and soil moisture (Figure 3b). Indeed,
35 performance metrics at the daily time scale show a large decline in the performance of HGS-PM during wet periods (NSE = 0.04) compared to dry periods (NSE = 0.64; Table 5). At the opposite, the performance of HGS-MEP was comparable for dry (NSE = 0.86) and wet periods (NSE = 0.85). Moreover, in-between monsoon periods, terrestrial evaporation was underestimated by HGS-PM (PBIAS = –14%; Table 4) and the model was unable to catch terrestrial evaporation pulses following rain events (e.g. 2013, Figure 3c). As a result, soil moisture was generally overestimated (PBIAS = 27%)
40 throughout the simulation period. At the diurnal scale, the HGS-MEP model reproduced well subdaily variations in terrestrial evaporation at US-Wkg, with an increase in the morning, peak value around 12:00, a decrease in the afternoon, and values close to zero during the night (Figure 5a). In the HGS-MEP simulation, the daily maximum was generally overestimated with an average of 0.12 mm h^{-1} at 12:00, compared to an observed average of 0.10 mm h^{-1}. On the other hand, morning and afternoon values were slightly underestimated, by about 0.01 mm h^{-1} (Figure 5a). While the HGS-PM did not overestimate

the daily maximum (Figure 5a), the HGS-MEP model overall outperformed HGS-PM for the simulation of half-hourly terrestrial evaporation, as shown by the four performance metrics (RMSE, NSE, R², PBIAS, Table 6).

Table 4. Performance of the HGS-MEP and HGS with Penman-Monteith (HGS-PM) models when simulating a) daily mean soil water content (SWC) at a 15- or 20-cm depth and b) daily mean total terrestrial evaporation (E) as represented by the root mean square error (RMSE), Nash-Sutcliffe Efficiency (NSE), benchmark efficiency (BE), coefficient of determination (R²) and percentage bias (PBIAS).

	RMSE		NSE		BE		R²		PBIAS	
	HGS-MEP	HGS-PM	HGS-MEP	HGS-PM	HGS-MEP	HGS-PM	HGS-MEP	HGS-PM	HGS-MEP	HGS-PM
a) SWC	(m^3 m^{-3})								(%)	
US-Wkg	0.04	0.05	0.30	–0.10	–0.35	–1.13	0.62	0.54	19	27
US-Ton	0.03	0.04	0.92	0.88	0.60	0.46	0.94	0.89	–5	0
US-WBW	0.05	0.05	0.61	0.51	–0.22	–0.54	0.74	0.66	–6	–1
b) E	(mm day^{-1})								(%)	
US-Wkg	0.31	0.58	0.88	0.57	0.48	–0.86	0.89	0.65	–10	–14
US-Ton	0.43	0.55	0.73	0.56	0.11	–0.45	0.77	0.70	–14	–25
US-WBW	0.71	0.74	0.65	0.62	–1.70	–1.93	0.68	0.69	11	–23

Table 5. Performance of the HGS-MEP and HGS with Penman-Monteith (HGS-PM) models when simulating daily mean total terrestrial evaporation (E) during dry and wet periods as represented by the root mean square error (RMSE), Nash-Sutcliffe Efficiency (NSE), coefficient of determination (R²) and percentage bias (PBIAS). n represents the number of days.

	n	RMSE		NSE		R²		PBIAS	
		HGS-MEP	HGS-PM	HGS-MEP	HGS-PM	HGS-MEP	HGS-PM	HGS-MEP	HGS-PM
		(mm day^{-1})						(%)	
US-Wkg									
dry (P/PET<0.4)	1518	0.29	0.46	0.86	0.64	0.87	0.68	–11	–15
wet (P/PET≥0.4)	308	0.39	0.98	0.85	0.04	0.83	0.47	–9	–12
US-Ton									
dry (P/PET<1)	1340	0.43	0.56	0.76	0.59	0.81	0.72	–14	–24
wet (P/PET≥1)	486	0.44	0.49	0.37	0.20	0.58	0.61	–10	–27
US-WBW									
dry (P/PET<1)	489	0.78	0.87	0.54	0.42	0.57	0.57	6	–23
wet (P/PET≥1)	425	0.61	0.54	0.57	0.66	0.65	0.71	26	–24

Table 6. Performance of the HGS-MEP and HGS with Penman-Monteith (HGS-PM) models when simulating half-hourly mean total terrestrial evaporation as represented by the root mean square error (RMSE), Nash-Sutcliffe Efficiency (NSE), coefficient of determination (R²) and percentage bias (PBIAS).

	RMSE		NSE		R²		PBIAS	
	HGS-MEP	HGS-PM	HGS-MEP	HGS-PM	HGS-MEP	HGS-PM	HGS-MEP	HGS-PM
	(mm h⁻¹)						(%)	
US-Wkg	0.05	0.06	0.65	0.48	0.72	0.58	3	–9
US-Ton	0.06	0.06	0.53	0.55	0.61	0.60	–3	–18
US-WBW	0.10	0.08	0.47	0.62	0.57	0.64	23	–18
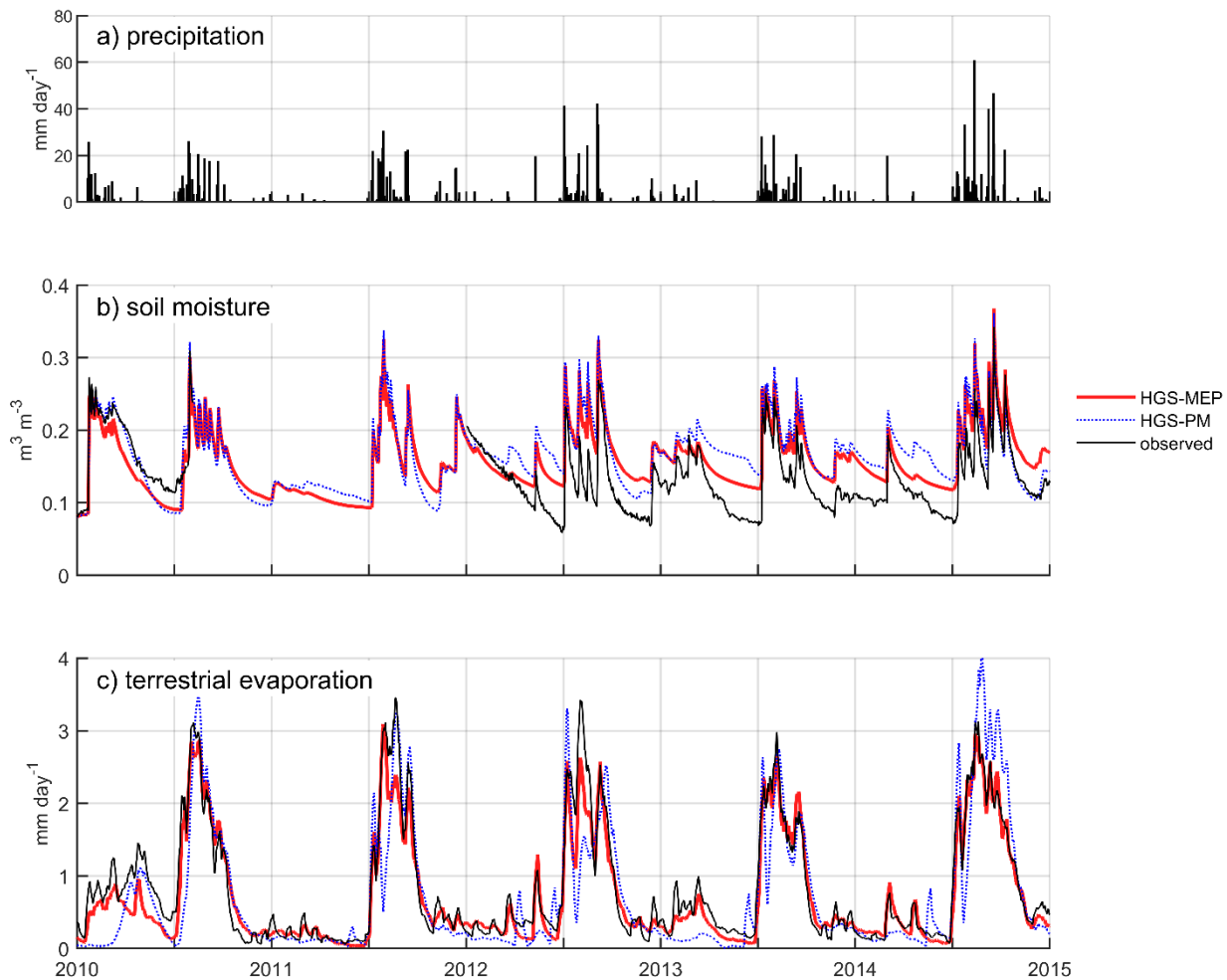
Figure 3. a) Precipitation, as well as observed and modeled b) daily mean soil water content at a depth of 15 cm and c) 10-day moving average of terrestrial evaporation at US-Wkg (climate: semiarid, vegetation: grassland).
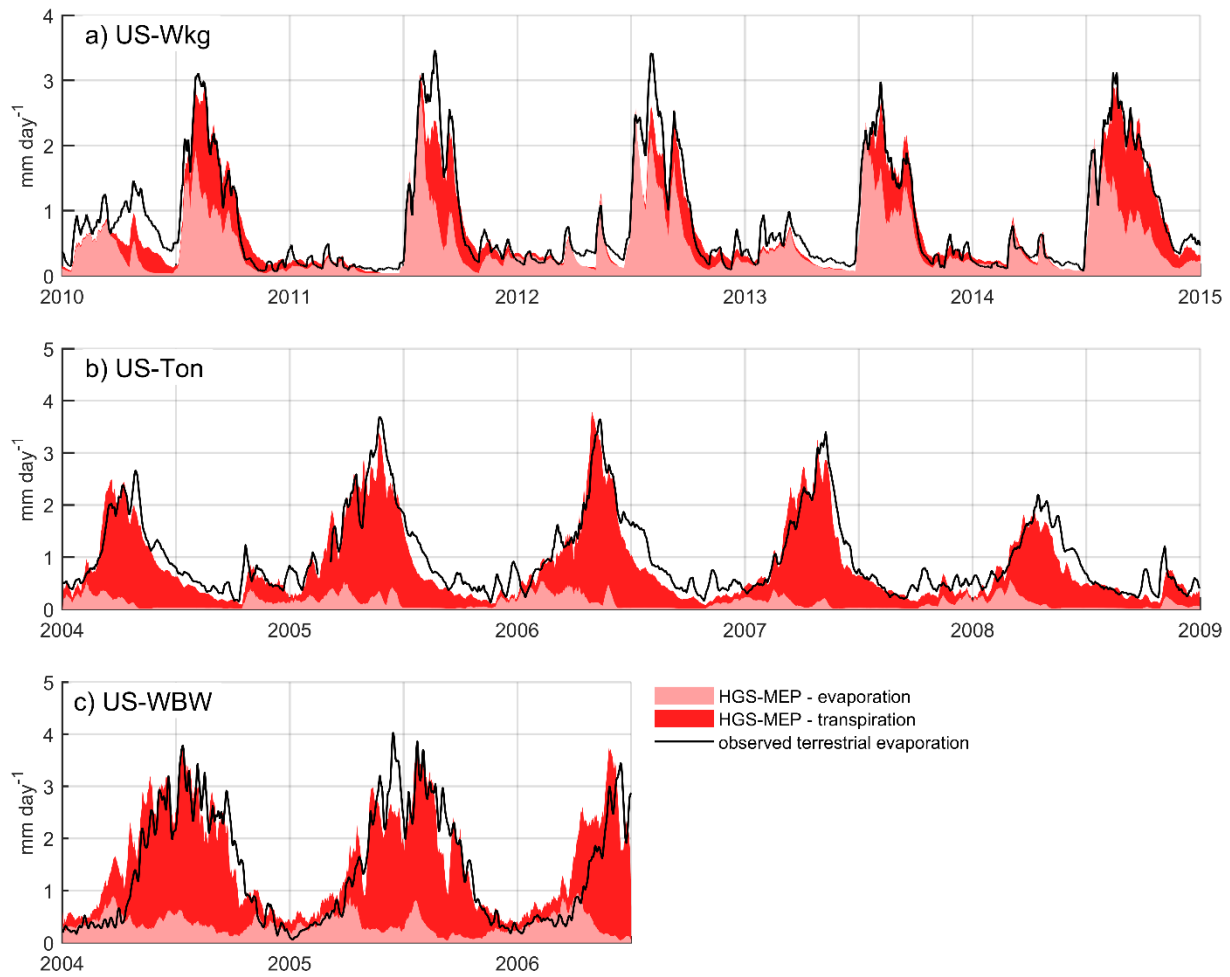
Figure 4. Ten-day moving average of observed terrestrial evaporation and modeled terrestrial evaporation partitioned as transpiration and evaporation at a) US-Wkg (climate: semiarid, vegetation: grassland), b) US-Ton (climate: Mediterranean, vegetation: woody savanna) and c) US-WBW (climate: temperate, vegetation: deciduous broadleaf forest).
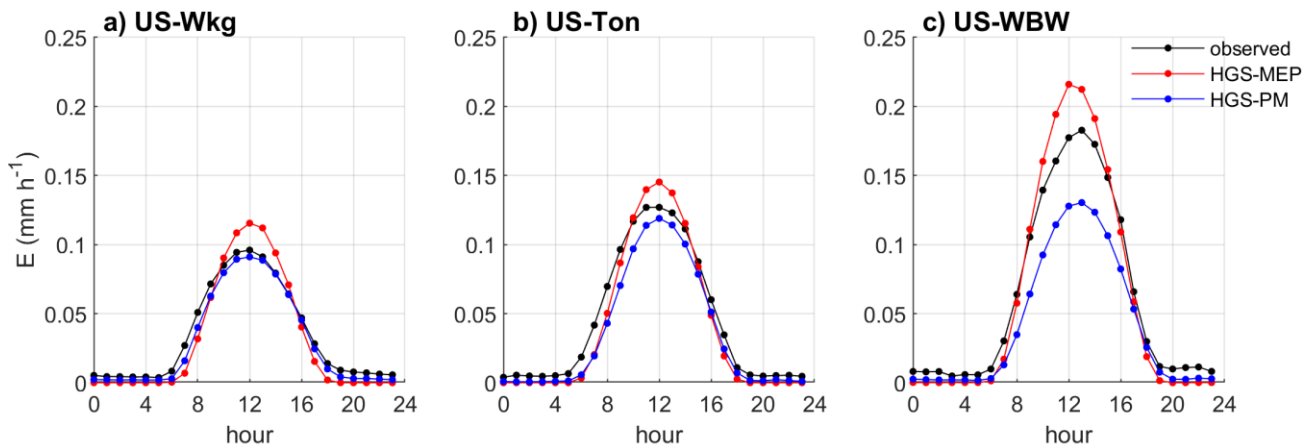
Figure 5. Observed and modeled hourly average terrestrial evaporation at US-Wkg (climate: semiarid, vegetation: grassland), b) US-Ton (climate: Mediterranean, vegetation: woody savanna) and c) US-WBW (climate: temperate, vegetation: deciduous broadleaf forest).

4.2 Model performance under a Mediterranean climate (US-Ton)

During the study period (2004–2008), mean annual precipitation at US-Ton ranged between 371 and 782 mm, with most precipitation concentrated during winter months from October to May (Figure 6a). The first two winters (2004–2005 and 2005–2006) of the study period were particularly wet (precipitation = 717 mm and 882 mm), while the following years experienced near-normal precipitation (385 mm and 392 mm). As shown in Figure 6b, the HGS-MEP model simulated soil moisture exceptionally well at a 20-cm depth (RMSE = 0.03 m^3 m^{-3}; NSE = 0.92; Table 4) and was able to reproduce the decrease in soil moisture as precipitation stops in summer (Figure 6b). During the wet winter months, the HGS-MEP model slightly underestimated soil moisture (PBIAS = –5%) but still captured the increase in soil moisture during this period. Near the surface (z = 0 cm, Figure S2a), soil moisture was generally underestimated by HGS-MEP during the dry summer months: observed soil water content slowly decreased until it generally reached a minimum of 0.04 – 0.05 m^3 m^{-3} at the end of the season, while modeled soil moisture dropped rapidly to reach a minimum value (0.03 m^3 m^{-3}) close to the residual water content (0.02 m^3 m^{-3}; Table 2). For the deeper soil layers (z = 50 cm), the HGS-MEP model generally overestimated soil moisture during dry summer months with a modeled minimum of 0.17 m^3 m^{-3} compared to an observed minimum of 0.14 m^3 m^{-3} (Figure S2c).

When simulating terrestrial evaporation , the HGS-MEP model performed well (RMSE = 0.43 mm day^{-1}; NSE = 0.73) although terrestrial evaporation was underestimated (PBIAS = –14%; Table 4). The HGS-MEP model performed particularly well for winter months and was able to capture the increase in terrestrial evaporation from about 0.4 mm day^{-1} (modeled average terrestrial evaporation in September) to 3.3 mm day^{-1} (modeled average annual maximum terrestrial evaporation) as water became more available. However, following those winter months, as precipitation stopped, terrestrial evaporation simulated by HGS-MEP was underestimated during the first half of the dry period (June – July). For example, the underestimation in terrestrial evaporation during the summer of 2005 and 2006 (i.e. from the last day of precipitation in May or June to the end of September) amounted respectively to a cumulative difference of 8.1 and 6.8 mm between observed and modeled terrestrial evaporation. During the dry summer months, low soil moisture availability near the surface (Figure S2a) limited evaporation simulated by HGS-MEP and modeled transpiration accounted on average for 94% of total terrestrial evaporation (Figure 4b). Evaporation increased during the monsoon period and, on average, terrestrial evaporation simulated by HGS-MEP was made up of 17% of evaporation and 83% of transpiration. Overall, the HGS-PM model performed well at US-Ton at a daily time scale, although the HGS-MEP performed slightly better. As opposed to HGS-MEP, the HGS-PM had difficulties capturing the onset of the wet winter period and the increase in soil moisture occurred ahead of time (Figure 6b). Indeed, we observed a decline in the performance of HGS-PM during wet periods (NSE = 0.20) compared to dry periods (NSE = 0.59; Table 5). We observed a similar pattern with HGS-MEP, but not as marked with a NSE of 0.37 during wet periods compared to 0.76 during dry periods (Table 5). With HGS-MEP and HGS-PM, terrestrial evaporation was underestimated, both during wet and dry periods (–27% ≤ PBIAS ≤ –10%, Table 5). This underestimation was particularly important in June and July when precipitation stopped (Figure 6c). At the diurnal scale, both models performed similarly well (NSE = 0.53 for HGS-MEP and NSE = 0.55 for HGS-PM), although HGS-PM led to a more important bias (PBIAS = –18%) than HGS-MEP (PBIAS = –3%; Table 6). Throughout the day, both models underestimated terrestrial evaporation in the morning and afternoon, while the daily maximum was generally overestimated by HGS-MEP and slightly underestimated by HGS-PM (Figure 5b).
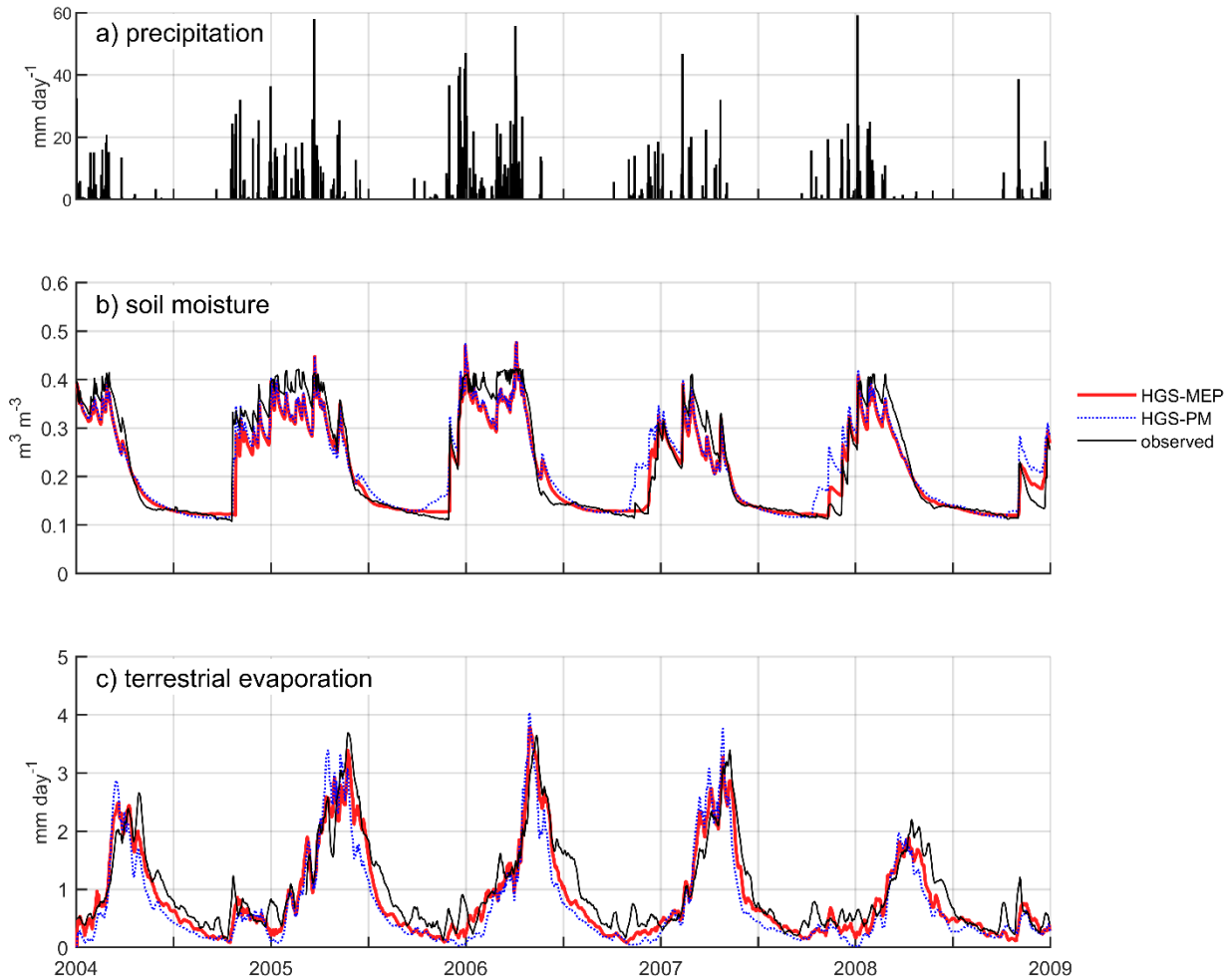
Figure 6. a) Precipitation, as well as observed and modeled b) daily mean soil water content at a depth of 20 cm and c) 10-day moving average of terrestrial evaporation at US-Ton (climate: Mediterranean, vegetation: woody savanna).

4.3 Model performance under a temperate climate (US-WBW)

In the simulation period, 2004 was a relatively wet year (annual precipitation = 1600 mm), while 2005 was relatively dry (annual precipitation = 995 mm; Figure 7a). In Figure 7b, the HGS-MEP model provided a realistic simulation of soil moisture (RMSE = 0.05 m^3 m^{-3}; NSE = 0.61; Table 4) and captured the decrease in soil moisture associated with increased vegetation activity during the summer. However, soil moisture at a 20 cm depth was generally overestimated by HGS-MEP during the summer and modeled soil water content did not fall below 0.1 m^3 m^{-3} while the observed soil water content reached an annual minimum of 0.08 m^3 m^{-3} and 0.05 m^3 m^{-3} in 2004 and 2005. At the opposite, soil moisture during the winter was generally underestimated by HGS-MEP with a modeled average soil water content of 0.21 m^3 m^{-3} between January and April in comparison with an observed average of 0.26 m^3 m^{-3}. Overall, a similar pattern (overestimation of soil moisture in the summer and underestimation in the winter) was observed in soil moisture simulations near the surface ($z = 5$ cm; Figure S3a). As for deeper soil layers ($z = 60$ cm), soil moisture was systematically underestimated, although this could be due to changes in soil properties given there is an upper shift in observed soil moisture values compared to upper soil layers (Figure S3c).

In Figure 7c, the HGS-MEP model performed well and reproduced the seasonal pattern in terrestrial evaporation (RMSE = 0.71 mm day^{-1}; NSE = 0.65; Table 4). Capturing the onset of vegetation activity was, however, challenging for the model and, early in the summer, terrestrial evaporation was generally overestimated (PBIAS = 11%). On two occasions, terrestrial

evaporation was considerably underestimated by the HGS-MEP model: in June 2005, observed terrestrial evaporation reached a peak of 3.9 mm day^{-1}, while modeled terrestrial evaporation was about 2.5 mm day^{-1} and in September 2005, observed terrestrial evaporation reached 2.8 mm day^{-1}, while modeled terrestrial evaporation went below 1 mm day^{-1} (values refer to the 10-day moving average presented in Figure 4c). This underestimation in terrestrial evaporation is linked to the

5   water stress factor. In both cases, the water stress factor fell below 0.5 for a few days, which largely reduced modeled transpiration. Evaporation simulated by HGS-MEP was relatively constant throughout the year with an average of 0.4 mm day^{-1}, although in the fall 2005, following a particularly dry summer, modeled evaporation dropped to less than 0.1 mm day^{-1}. Transpiration simulated by HGS-MEP accounted on average for 57% of total terrestrial evaporation between October and April, but this proportion increased considerably during the summer. Indeed, between May and September, modeled

10   transpiration represented on average 87% of total terrestrial evaporation. Overall, the HGS-MEP model outperformed HGS-PM, although, as shown by negative BE values, both models had less explanatory power than a simple benchmark model that captures seasonality. The two models performed similarly during dry and wet periods, with only a slight decline in performance at HGS-PM during dry periods in the summer (NSE = 0.42) compared to wet periods in the winter (NSE = 0.66; Table 5). During summer months, the HGS-PM largely underestimated terrestrial evaporation (PBIAS = –23%), particularly

15   during the dry 2005 year (Figure 7c). As a result, soil moisture was overestimated by HGS-PM, and much more so than with HGS-MEP (Figure 7b). During winter months, soil moisture was generally underestimated, although a similar pattern was observed for HGS-MEP. At the diurnal scale, the HGS-PM (NSE = 0.62) performed better than HGS-MEP (NSE = 0.47) when simulating half-hourly terrestrial evaporation, although both models had an important bias, positive for HGS-MEP (PBIAS = 23%) and negative for HGS-PM (PBIAS = –18%; Table 6). This bias is particularly reflected in the simulation of

20   the daily maximum which was overstimated by HGS-MEP and largely underestimated by HGS-PM (Figure 5c). Indeed, the daily maximum observed mid-day at US-WBW is 0.18 mm h^{-1}, while it reached 0.22 mm h^{-1} with HGS-MEP and 0.13 mm h^{-1} with HGS-PM.
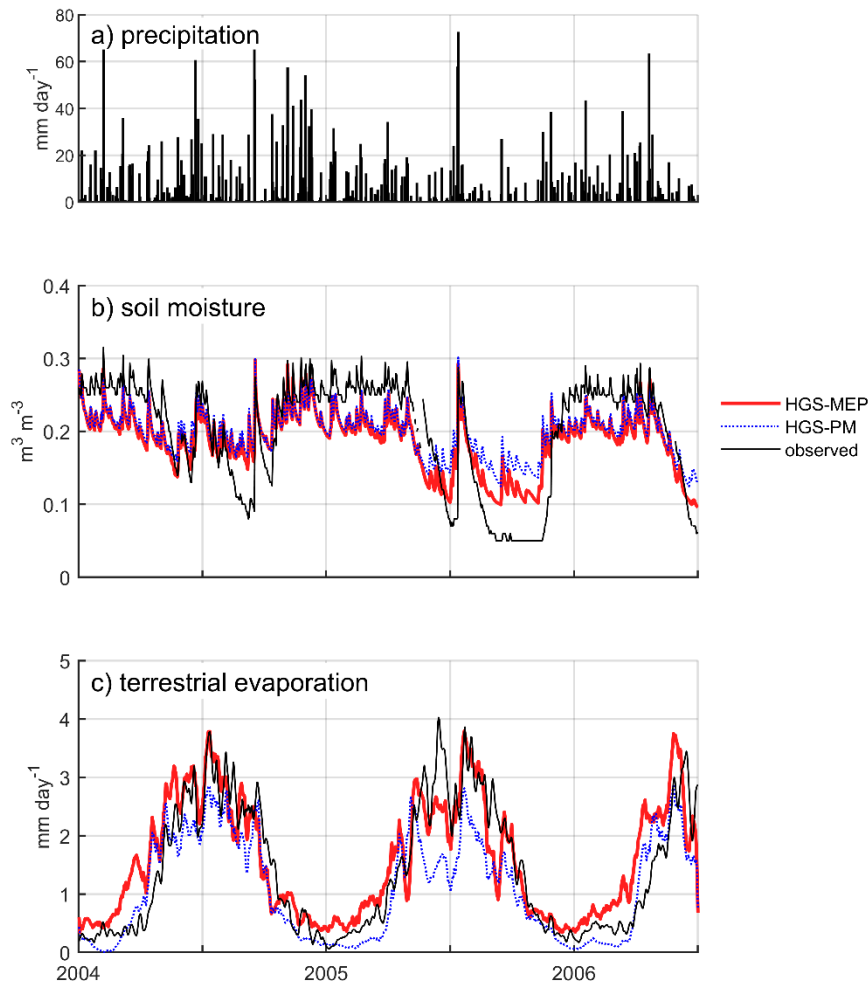
Figure 7. a) Precipitation, as well as observed and modeled b) daily mean soil water content at a depth of 20 cm and c) 10-day moving average of terrestrial evaporation at US-WBW (climate: temperate, vegetation: deciduous broadleaf forest).

5 Discussion

5.1 Performance of the HGS-MEP model

5.1.1 HGS-MEP vs HGS-PM

At the daily time scale, the HGS-MEP model outperformed HGS-PM when simulating terrestrial evaporation at the three study sites, which translated into improved performance for soil moisture modeling as well (Table 4). Notably, we observed a weak performance of HGS-PM during wet periods at US-Wkg (P/PET≥0.4) and US-Ton (P/PET≥1; Table 5). At US-Wkg, this meant that HGS-PM failed to capture the annual maximum terrestrial evaporation which has important implications for the water budget. At the opposite, the weaker performance at US-Ton by HGS-PM, and to a lesser degree by HGS-MEP, meant that the two models struggle to describe the minimum rates of terrestrial evaporation. At US-WBW, both models had a comparable performance with consistent results for HGS-MEP for wet (P/PET≥1) and dry periods, while HGS-PM performed better during wet periods than dry periods (Table 5).

At the semiarid site US-Wkg (Figure 3), a better handling of terrestrial evaporation partitioning can explain the superior performance of HGS-MEP compared to HGS-PM, at both daily and half-hourly time scales. Indeed, the HGS-MEP model

assesses transpiration and evaporation independently one from another. In the Kristensen and Jensen (1975) model in HGS, transpiration and evaporation are instead derived from a single PET value, although we could realistically expect potential transpiration and evaporation to differ from one another. In fact, Shuttleworth and Wallace (1985) have proposed a two-layer configuration of the Penman-Monteith model which allows the definition of different resistance values for the soil and canopy layers. However, HGS remains limited to the definition of a single PET value at the moment. We encountered a large overestimation of terrestrial evaporation when deriving transpiration and evaporation from a single PET value and we set up the HGS model to only allow bare soil evaporation in the absence of active vegetation ($f_1(LAI) = 0$). As a result, the HGS-PM model performed weakly at US-Wkg, where soil evaporation makes up more than 50% of terrestrial evaporation according to observations (Moran et al., 2009). Soil moisture modeling by HGS-MEP also proved somewhat challenging at US-Wkg (NSE = 0.30, BE = –0.35; Table 4). However, in the absence of parameter calibration, we consider this performance more than acceptable given the challenges of modeling water fluxes under arid climates. Soil moisture was generally overestimated by HGS-MEP during dry periods (Figure 3) and further work on the definition of the wilting point in arid climates could help improve the performance of the model. Indeed, wilting can occur at a lower threshold than –1.5 MPa (–4 to –2 MPa, Baldocchi et al., 2004) for vegetation having evolved under an arid climate.

At the Mediterranean site US-Ton, daily terrestrial evaporation was underestimated by HGS-MEP (PBIAS = –14%, Table 4), particularly during the second half of the year, as reduced water supply led to a decline in terrestrial evaporation (Figure 5). While the HGS-MEP model simulates soil moisture very well at a depth of 20 cm (Figure 6), it tended to underestimate soil moisture close to the surface (Figure S2a), where the largest proportion of roots is found according to the vertical root distribution defined by HGS (cubic decay distribution between the surface and the maximum root depth). Given that the water stress factor (η_s) is computed from the weighted average soil water content over the root zone (equation 12), this underestimation of soil moisture near the surface translated into an overestimation of the reduction in transpiration resulting from water stress. We also investigated if the issue of water stress overestimation could be due to a misdefinition of the maximum rooting depth, as trees under a Mediterranean climate have been found to access water from deep soil layers or groundwater (Miller et al., 2010). However, we also simulated terrestrial evaporation with the stand-alone MEP model using soil moisture observations, thus avoiding the overestimation of water stress near the surface, and instead found a large overestimation of terrestrial evaporation (Figure S4). These results suggest that increasing the rooting depth to increase access to water resources would likely not improve the simulation of terrestrial evaporation. Instead, uncertainty relative to the definition of the vertical root distribution (as opposed to the maximum rooting depth) or, as previously discussed, with the definition of water stress points (wilting point and field capacity) may explain the challenge of simulating terrestrial evaporation under water-limited conditions at US-Ton.

At the half-hourly time scale, both HGS-MEP and HGS-PM showed lower performance than at a daily time scale when simulating terrestrial evaporation. For example, the NSE varied between 0.56 and 0.88 at a daily time scale (Table 4), while it varied between 0.47 and 0.65 at a half-hourly time scale (Table 6). At a half-hourly time scale, no model is distinctly superior from one another: HGS-MEP performed better at US-Wkg, HGS-PM performed better at US-WBW and both models performed similarly at US-Ton (Table 6). Still, we observed a distinct pattern where peak terrestrial evaporation during the day was generally overestimated by HGS-MEP and underestimated by HGS-PM (Figure 5). A known issue of energy imbalance, particularly at subdaily time scales, is associated with eddy covariance measurements (Leuning et al., 2012). This issue typically leads to an underestimation in observations of terrestrial evaporation and could in part explain the apparent issue of overestimation of peak values by HGS-MEP. On the other hand, the negative bias of HGS-PM at the half-hourly time scale ($–18\% \leq$ PBIAS $\leq –9\%$; Table 6) may actually be even more important when taking into account the energy imbalance issue.

Overall, the predictive ability of the MEP model is particularly noteworthy given that we did not rely on calibration and instead used a priori estimation of parameters describing the soil and vegetation. The MEP model thus offers a promising alternative to model hydrologic fluxes without relying on calibration (Wagener, 2007). We chose the Penman-Monteith as a benchmark against which to compare the MEP model as it is a physically based model that allows for a detailed

parameterization of vegetation. However, studies have shown that the Penman-Monteith leads to an underestimation of terrestrial evaporation under a contemporary climate (Ershadi et al., 2014) and an overestimation under climate change (Milly and Dunne, 2016). Other models could have been considered, although Hajji et al. (2018) demonstrated the superior performance of the MEP model compared to other models such as the modified Priestley-Taylor-Jet Propulsion Laboratory
5   (PT-JPL) and the air-relative-humidity-based two-source model (ARTS).

5.1.2 HGS-MEP vs HGS using observed terrestrial evaporation as a forcing

Maheu et al. (2018) assessed HGS' skills to model soil moisture at the same AmeriFlux sites used in the present study. In Maheu et al. (2018) and the present study, the same input values were used to define soil and vegetation properties. Both studies also considered the same periods, with the exception of the Mediterranean site (US-Ton) where simulations were
10 performed for different periods (2004-2008 in the present study vs 2008-2012 in Maheu et al., 2018) due to data availability. When modelling soil moisture with HGS, Maheu et al. (2018) used observed terrestrial evaporation as a forcing, thus reducing the uncertainty of simulating this flux and focusing the assessment of the model on subsurface processes and properties that control soil water content. These simulations thus offer a benchmark against which to compare the results of the present study and assess how much uncertainty is introduced by the simulation of terrestrial evaporation by the MEP
15 model. At the three sites, the HGS simulations of soil moisture that used observed terrestrial evaporation as a forcing performed slightly better than simulations with HGS-MEP. Still, the performance was overall comparable between HGS with observed terrestrial evaporation (RMSE = 0.04 m^3 m^{-3} and NSE between 0.39 and 0.86) and HGS-MEP (RMSE between 0.03 and 0.05 m^3 m^{-3} and NSE between 0.30 and 0.92). At the semiarid site (US-Wkg), the HGS-MEP simulation of soil moisture had a greater overestimation bias (19%, Table 4) than the HGS simulation (10%, Table 4 in Maheu et al., 2018),
20 which could be due to the underestimation of peak (2011 and 2012) or pre-monsoon (2010, 2012 and 2013) terrestrial evaporation (Figure 3). At the temperate site (US-WBW), simulations with HGS-MEP and HGS in Maheu et al. (2018) both showed the same pattern of underestimation of soil moisture in the winter and overestimation in the summer. This suggests that these biases are in good part associated with the definition of soil (hydraulic parameters) or vegetation (root distribution) properties rather than with the MEP model itself.

5.1.3 Partitioning of total terrestrial evaporation by HGS-MEP

In the present study, evaporation simulated by HGS-MEP represented on average 60% of total terrestrial evaporation at the semiarid site (US-Wkg) during the monsoon period (Figure 4a). These results are in line with experimental results from Moran et al. (2009) who estimated that, following the Lehmann lovegrass invasion, evaporation accounted for 55% of the total terrestrial evaporation during the growing season of a year with average precipitation. Results from the present study are
30 also concordant with those of Scott and Biederman (2017) who found that, on average, evaporation represented 54% of growing-season total terrestrial evaporation at US-Wkg between 2004 and 2015. Using overstory and understory flux tower measurements at the Mediterranean site US-Ton, Miller et al. (2010) found that transpiration from trees dominate during the dry summer months and that understory evaporation (i.e. bare soil evaporation and transpiration from grasses and forbs) is close to zero. Our results are consistent with these observations and according to the HGS-MEP simulation, transpiration
35 accounted on average for 94% of total terrestrial evaporation (Figure 4b). At the temperate site (US-WBW), soil evaporation, as measured by an understory flux tower, accounted for 16% of total terrestrial evaporation on an annual basis and for generally less than 8% of total terrestrial evaporation during the growing season (Wilson et al., 2001). In the present study, soil evaporation simulated by HGS-MEP amounted to 13% of total terrestrial evaporation during the growing season between May and September (Figure 4c), which agrees with these experimental estimates. Overall, the HGS-MEP model showed a
40 good capability for the partitioning of total terrestrial evaporation under various climates (semiarid, Mediterranean and temperate); a conclusion that was also reached for a humid, energy-limited environment (Wang et al., 2017).

5.2 Using the MEP model to integrate the energy budget in hydrological modeling: strengths and limitations

The MEP model of land surface fluxes offers an effective means to implement coupled water and energy budget modeling for hydrological applications. First, the MEP model of terrestrial evaporation requires six input variables: net radiation, soil surface temperature, leaf surface temperature and specific humidity, vegetation index as well as soil water content, the latter which can be supplied by a hydrological model. Thus, the MEP model eliminates the need for wind speed and surface roughness (input to the Penman model) or for vertical gradients of temperature and humidity (inputs to the aerodynamic method often implemented in land surface models). Second, the MEP model ensures, by design, the closure of the energy balance. As such, terrestrial evaporation simulated by the MEP model is constrained by available energy, which avoids issues of overestimation associated with the use of temperature-based PET models for hydrological projection. Third, the MEP model relies on a small set of equations making it straightforward to implement with minimal computational needs. Land surface models also offer a means of implementing coupled water and energy budget modeling but, contrary to the MEP model, these models are generally complex and computationally heavy. Last, the explicit partitioning of total terrestrial evaporation into evaporation and transpiration is also a strength of the MEP model given that water feeding these two fluxes are drawn from different pools. Partitioning has particularly important implications for terrestrial evaporation modeling under water-limiting conditions (e.g. arid environments, Kurc and Small, 2004) or under changing land cover conditions (Huxman et al., 2005) and the MEP model thus offers a tool to better represent these conditions in hydrological modeling.

While these four highlighted features make the MEP model a promising approach to couple water and energy budget modeling, certain limitations also need to be considered. First, the MEP model has mainly been tested with input data at a half-hourly time step. Although meteorological and climate data are increasingly available at a subdaily time step with the continuing increase in the temporal resolution of reanalysis and climate projection datasets, additional tests would be needed to assess the applicability of the MEP model at a daily time scale. Second, soil water content is the key coupling variable between the MEP and hydrological models, which limits the choice of hydrological models to which the MEP model can be coupled to. For the moment, the choice of a hydrological model appears limited to physical models, with the drawback that these models are often computationally intensive as well as challenging in terms of parameterization. Indeed, the simulation time for the one-dimensional soil columns in this study was greater than an hour with the HGS-MEP model. HGS is a relatively complex model and the MEP model has also been coupled to a soil moisture force-restore model with satisfying results (Huang and Wang, 2016, bias < 0.01 m^3 m^{-3} and R^2 = 0.81). As for conceptual hydrological models, further investigation is needed to assess the possibility of a coupling with the MEP model. In the absence of information on soil water content, a method would be needed to derive the specific humidity at the soil surface (q_{ss}) as well as the water stress factor (η_s) from the subsurface storage component of the conceptual model. Third, in its current form, the HGS-MEP model is still driven by dependent variables. For example, both net radiation and surface temperature are inputs to the model although incoming longwave radiation, a component of net radiation, is largely dependent on air temperature (used as a proxy for surface temperature T_{ls}). Moreover, soil surface temperature (T_{ss}) is an input to the model even though it is a function of the heat fluxes predicted by the model. In the present project, we have focused on the coupling of water fluxes between HGS and MEP although, in the future, the two models could also be more closely coupled since thermal transport modeling is implemented within HGS (Brookfield et al., 2009). In addition to soil moisture information, the HGS model could supply information on soil surface temperature to the MEP model and thus eliminate its need as an input variable. For example, Huang and Wang (2016) simulated surface soil temperature and moisture using a force-restore model that relies on the MEP model to simulate the heat budget.

6 Conclusion

Using the MEP model of land surface fluxes, we proposed a simple approach to integrate energy budget modeling in hydrological models in order to improve the simulation of terrestrial evaporation. The MEP model requires six input variables (net radiation, soil surface temperature and specific humidity, leaf surface temperature and specific humidity and vegetation index) and ensures energy budget closure, which imparts a strong physical basis and avoids issues of

oversensitivity to air temperature associated with certain PET models. We coupled the MEP model to HGS, an integrated surface and subsurface hydrologic model. Without calibration, the coupled HGS-MEP model performed well in simulating soil water content and terrestrial evaporation at three AmeriFlux sites with varying climates (semiarid, Mediterranean, temperate). For both the simulation of daily soil moisture and terrestrial evaporation, HGS-MEP outperformed the standalone
5 HGS model where, as defined by the Kristensen and Jensen (1975) model, terrestrial evaporation is derived from potential evaporation which we computed using the Penman-Monteith equation. Overall, results indicate that, through a simple coupling procedure, the MEP model offers a physically constrained approach to simulate terrestrial evaporation in hydrological models. This approach may offer a tool to better assess climate change impacts on water resources, although the predictive ability of the MEP model under environmental change, may it be natural (e.g. wildfires) or anthropogenic (e.g.
10 land cover change, climate change), still needs to be assessed. This study focused on the simulation of vertical water fluxes but, to use HGS-MEP for flow simulation and projection, lateral fluxes will need to be considered in further work. Various routing models are available and could be used in conjunction with HGS-MEP to simulate lateral fluxes in a computationally efficient way. Finally, the present study focused on the application of the HGS-MEP model at snow-free sites and the MEP model has undergone little testing in cold regions, with tests limited to the snow-free period (Wang et al., 2017). A MEP
15 model for snow surfaces (Wang et al., 2014) is available and could also be integrated to hydrological models to allow energy budget modeling throughout the year in northern environments.

Data availability

Data are available upon request from the corresponding author. For AmeriFlux data, see Baldocchi (2016), Meyers (2016) and Scott (2016).

20 **Supplement**

A Supplement related to this article is available.

Acknowledgements

This research was supported by NSERC (grants RDC/477125-14 and RGPIN/04892-2015), Hydro-Québec, Ouranos, and Environment and Climate Change Canada. We thank Dr. Jingfeng Wang (Georgia Tech) for his help with the implementation
25 of the MEP model. Funding for AmeriFlux data resources was provided by the U.S. Department of Energy's Office of Science. We thank the primary investigators of the AmeriFlux sites that made this research possible by making their data available: Russel Scott (US-Wkg), Dennis Baldocchi (US-Ton) and Tilden Meyers (US-WBW). All data used in this paper are listed in the tables and references.

References

30 Alves M, Music B, Nadeau DF, Anctil F. Comparing the Performance of the Maximum Entropy Production Model With a Land Surface Scheme in Simulating Surface Energy Fluxes. J. Geophys. Res.-Atmos 124 (6): 3279–3300 DOI: 10.1029/2018JD029282, 2019.

Andréassian, V., Perrin, C., and Michel, C.: Impact of imperfect potential evapotranspiration knowledge on the efficiency and parameters of watershed models. J. Hydrol., 286, 19–35, https://doi.org/10.1016/j.jhydrol.2003.09.030, 2004.

35 Aquanty.: HydroGeoSphere User Manual - release 1.0. Aquanty Inc, Waterloo, Canada, 2013.

Bae, D. H., Jung, I. W., and Lettenmaier, D. P.: Hydrologic uncertainties in climate change from IPCC AR4 GCM simulations of the Chungju Basin, Korea. J. Hydrol., 401(1–2), 90–105, https://doi.org/10.1016/j.jhydrol.2011.02.012, 2011.

Baldocchi, D.: AmeriFlux US-Ton Tonzi Ranch, https://doi.org/10.17190/AMF/1245971, 2016.

5   Baldocchi, D. D., Xu, L., and Kiang, N.: How plant functional-type, weather, seasonal drought, and soil physical properties alter water and energy fluxes of an oak-grass savanna and an annual grassland. Agr. Forest Meteorol., 123(1–2), 13–39, https://doi.org/10.1016/j.agrformet.2003.11.006, 2004.

Baldocchi, D. D., Falge, E., Gu, L., Olson, R., Hollinger, D., Running, S., et al.: FLUXNET : A new tool to study the temporal and spatial variability of ecosystem-scale carbon dioxide, water vapor, and energy flux densities. B. Am. 10   Meteorol. Soc., 82(11), 2415–2434, 2001.

Breshears, D. D., Adams, H. D., Eamus, D., McDowell, N. G., Law, D. J., Will, et al.: The critical amplifying role of increasing atmospheric moisture demand on tree mortality and associated regional die-off. Front. Plant Sci., 4, 266, https://doi.org/10.3389/fpls.2013.00266, 2013.

Brookfield, A. E., Sudicky, E. A., Park, Y.-J., and Conant Jr., B.: Thermal transport modeling in a fully integrated 15   surface/subsurface framework. Hydrol. Process., 23, 2150–2164, https://doi.org/10.1002/hyp.7282, 2009.

Brutsaert, W.: Evaporation into the atmosphere: Theory, history and applications, Springer, Dordrecht, 1982.

Dewar, R. C.: Maximum entropy production and the fluctuation theorem. J. Phys. A-Math. Gen., 38(21), L371–L381, https://doi.org/10.1088/0305-4470/38/21/L01, 2005.

Dewar, R. C.: Maximum entropy production as an inference algorithm that translates physical assumptions into macroscopic 20   predictions: Don't shoot the messenger. Entropy, 11, 931–944, https://doi.org/10.3390/e11040931, 2009.

Donohue, R. J., Mcvicar, T. R., and Roderick, M. L.: Assessing the ability of potential evaporation formulations to capture the dynamics in evaporative demand within a changing climate. J. Hydrol., 386, 186–197, https://doi.org/10.1016/j.jhydrol.2010.03.020, 2010.

Ehret, U., Gupta, H. V., Sivapalan, M., Weijs, S. V., Schymanski, S. J., Blöschl, G., et al.: Advancing catchment hydrology 25   to deal with predictions under change. Hydrol. Earth Syst. Sc., 18, 649–671, https://doi.org/10.5194/hess-18-649-2014, 2014.

Ekström, M., Jones, P. D., Fowler, H. J., Lenderink, G., Buishand, T. A., and Conway, D.: Regional climate model data used within the SWURVE project 1: projected changes in seasonal patterns and estimation of PET. Hydrol. Earth Syst. Sc., 11(3), 1069–1083, https://doi.org/10.5194/hess-11-1069-2007, 2007.

30   Ershadi, A., McCabe, M. F., Evan, J. P., Chaney, N. W., and Wood, E. F.: Multi-site evaluation of terrestrial evaporation models using FLUXNET data, Agr. Forest Meteorol., 187, 46–61, https://doi.org/10.1016/j.agrformet.2013.11.008, 2014.

Feddes, R. A., Kowalik, P. J., and Zaradny, H.: Simulation of field water use and crop yield, John Wiley and Sons, New York, 1978.

35   Ferguson, I. M., Jefferson, J. L., Maxwell, R. M., and Kollet, S. J.: Effects of root water uptake formulation on simulated water and energy budgets at local and basin scales. Environ. Earth Sci., 75, 316, https://doi.org/10.1007/s12665-015-5041-z, 2016.

Ficklin, D. L., and Novick, K. A.: Historic and projected changes in vapor pressure deficit suggest a continental-scale drying of the United States atmosphere. J. Geophys. Res., 122(4), 2061–2079, https://doi.org/10.1002/2016JD025855, 2017.

5   Gaborit, É., Fortin, V., Xu, X., Seglenieks, F., Tolson, B., Fry, L. M., et al.: A hydrological prediction system based on the SVS land-surface scheme: efficient calibration of GEM-Hydro for streamflow simulation over the Lake Ontario basin. Hydrol. Earth Syst. Sc., 21, 4825–4839, https://doi.org/10.5194/hess-21-4825-2017, 2017.

Gibbens, R., and Lenz, J.: Root system of some Chihuhuan Desert plants. J. Arid Environ., 49, 221–263, 2001.

Gutman, G., and Ignatov, A.: The derivation of the green vegetation fraction from NOAA / AVHRR data for use in numerical weather prediction models. Int. J. Remote Sens., 19(8), 1533–1543, https://doi.org/10.1080/014311698215333, 10   1998.

Hajji, I., Nadeau, D. F., Music, B., Anctil, F., Wang, J.: Application of the maximum entropy production model of evapotranspiration over partially vegetated water-limited land surfaces. J. Hydrometeorol., 19, 989–1005, 2018.

Hamon, W.: Computation of direct runoff amounts from storm rainfall. International Association of Scientific Hydrology, 63, 52–62, 1963.

15   Hird, J. N., and McDermid, G. J.: Noise reduction of NDVI time series: An empirical comparison of selected techniques. Remote Sens. Environ., 113, 248–258, https://doi.org/10.1016/j.rse.2008.09.003, 2009.

Hobbins, M. T., Dai, A., Roderick, M. L., and Farquhar, G. D.: Revisiting the parameterization of potential evaporation as a driver of long-term water balance trends. Geophys. Res. Lett., 35(12), 1–6, https://doi.org/10.1029/2008GL033840, 2008.

20   Hoerling, M. P., Eischeid, J. K., Quan, X.-W., Diaz, H. F., Webb, R. S., Dole, R. M., and Easterling, D. R.: Is a transition to semipermanent drought conditions imminent in the U.S. Great Plains? J. Climate, 25(24), 8380–8386, https://doi.org/10.1175/JCLI-D-12-00449.1, 2012.

Hosseinzadehtalaei, P., Tabari, H., and Willems, P.: Quantification of uncertainty in reference evapotranspiration climate change signals in Belgium. Hydrol. Res., 1–13, https://doi.org/10.2166/nh.2016.243, 2016.

25   Huang, S.-Y., and Wang, J.: A coupled force-restore model of surface temperature and soil moisture using the maximum entropy production model of heat fluxes. J. Geophys. Res.-Atmos., 121, 7528–7547, https://doi.org/10.1002/2015JD024586, 2016.

Huxman, T. E., Wilcox, B. P., Breshears, D. D., Scott, R. L., Snyder, K. A., Small, E. E., et al.: Ecohydrological implications of woody plant encroachment. Ecology, 86(2), 308–319, 2005.

30   Ichii, K., Wang, W., Hashimoto, H., Yang, F., Votava, P., Michaelis, A. R., and Nemani, R. R.: Refinement of rooting depths using satellite-based evapotranspiration seasonality for ecosystem modeling in California. Agr. Forest Meteorol., 149, 1907–1918, https://doi.org/10.1016/j.agrformet.2009.06.019, 2009.

Isabelle, P.-E., Nadeau, D., Rousseau, A., and Anctil, F.: Water budget, performance of evapotranspiration formulations, and their impact on hydrological modeling of a small boreal peatland-dominated watershed. Can. J. Earth Sci., 55(2), 35   206-220, https://doi.org/10.1139/cjes-2017-0046, 2018.

Jaynes, E. T.: Information theory and statistical mechanics. Phys. Rev., 106, 620–630, https://doi.org/10.1103/PhysRev.106.620, 1957.

Kay, A. L., and Davies, H. N.: Calculating potential evaporation from climate model data: A source of uncertainty for hydrological climate change impacts. J. Hydrol., 358(3–4), 221–239, https://doi.org/10.1016/j.jhydrol.2008.06.005, 2008.

Kingston, D. G., Todd, M. C., Taylor, R. G., Thompson, J. R., and Arnell, N. W.: Uncertainty in the estimation of potential evapotranspiration under climate change. Geophys. Res. Lett., 36(20), 3–8, https://doi.org/10.1029/2009GL040267, 2009.

Kleidon, A., and Schymanski, S.: Thermodynamics and optimality of the water budget on land: A review. Geophys. Res. Lett., 35, L20404. https://doi.org/ 10.1029/2008GL035393, 2008.

Koch, J., Cornelissen, T., Fang, Z., Bogena, H., Diekkrüger, B., Kollet, S., and Stisen, S.: Inter-comparison of three distributed hydrological models with respect to seasonal variability of soil moisture patterns at a small forested catchment. J. Hydrol., 533, 234–249, https://doi.org/10.1016/j.jhydrol.2015.12.002, 2016.

Koedyk, L. P., and Kingston, D. G.: Potential evapotranspiration method influence on climate change impacts on river flow: a mid-latitude case study. Hydrol. Res., 951–963, https://doi.org/10.2166/nh.2016.152, 2016.

Kristensen, K. J., and Jensen, S. E.: A model for estimating actual evapotranspiration from potential evapotranspiration. Nord. Hydrol., 6, 170–188, https://doi.org/10.2166/nh.1975.012, 1957.

Kumar, A., Chen, F., Niyogi, D., Alfieri, J. G., Ek, M., and Mitchell, K.: Evaluation of a photosynthesis-based canopy resistance formulation in the Noah land-surface model. Bound.-Lay. Meteorol., 138(2), 263–284, https://doi.org/10.1007/s10546-010-9559-z, 2011.

Kunstmann, H., Jung, G., Wagner, S., and Clottey, H.: Integration of atmospheric sciences and hydrology for the development of decision support systems in sustainable water management. Phys. Chem. Earth, 33(1–2), 165–174, https://doi.org/10.1016/j.pce.2007.04.010, 2008.

Kurc, S. A., and Small, E. E.: Dynamics of evapotranspiration in semiarid grassland and shrubland ecosystems during the summer monsoon season, central New Mexico. Water Resour. Res., 40(9), 1–15, https://doi.org/10.1029/2004WR003068, 2004.

Leuning R, van Gorsel E, Massman WJ, Isaac PR. Reflections on the surface energy imbalance problem. Agr. Forest Meteorol 156: 65–74 DOI: 10.1016/j.agrformet.2011.12.002, 2012.

Livneh, B., Restrepo, P. J., and Lettenmaier, D. P.: Development of a unified land model for prediction of surface hydrology and land–atmosphere interactions. J. Hydrometeorol., 12(6), 1299–1320, https://doi.org/10.1175/2011JHM1361.1, 2011.

Lofgren, B. M., Hunter, T. S., and Wilbarger, J.: Effects of using air temperature as a proxy for potential evapotranspiration in climate change scenarios of Great Lakes basin hydrology. J. Great Lakes Res., 37(4), 744–752, https://doi.org/10.1016/j.jglr.2011.09.006, 2011.

Maheu, A., Anctil, F., Gaborit, E., Fortin, V., Nadeau, D.F., Therrien, R.: A field evaluation of soil moisture modeling with the Soil, Vegetation, and Snow (SVS) land surface model using evapotranspiration observations as forcing data. J. Hydrol., 558, 532-545, https://doi.org/10.1016/j.jhydrol.2018.01.065, 2018.

Maxwell, R., and Miller, N.: Development of a coupled land surface and groundwater model. J. Hydrometeorol., 6(3), 233–247, https://doi.org/10.1175/JHM422.1, 2005.

Maxwell, R., Putti, M., Meyerhoff, S., Delfs, J., Ferguson, I., Ivanov, V., et al.: Surface-subsurface model intercomparison: a first set of benchmark results to diagnose integrated hydrology and feedbacks. Water Resour. Res., 50, 1531–1549, https://doi.org/10.1002/2013WR013725, 2014.

McAfee, S. A.: Methodological differences in projected potential evapotranspiration. Climatic Change, 120(4), 915–930, https://doi.org/10.1007/s10584-013-0864-7, 2013.

McKenney, M. S., and Rosenberg, N. J.: Sensitivity of some potential evapotranspiration estimation methods to climate change. Agr. Forest Meteorol., 64, 81–110, https://doi.org/10.1016/0168-1923(95)02239-T, 1993.

McMahon, T. A., Peel, M. C., and Karoly, D. J.: Assessment of precipitation and temperature data from CMIP3 global climate models for hydrologic simulation. Hydrol. Earth Syst. Sc., 19(1), 361–377, https://doi.org/10.5194/hess-19-361-2015, 2015.

McVicar, T. R., Van Niel, T. G., Li, L. T., Roderick, M. L., Rayner, D. P., Ricciardulli, L., and Donohue, R. J.: Wind speed climatology and trends for Australia, 1975-2006: Capturing the stilling phenomenon and comparison with near-surface reanalysis output. Geophys. Res. Lett., 35(20), 1–6, https://doi.org/10.1029/2008GL035627, 2008.

Meyers, T.: AmeriFlux US-WBW Walker Branch Watershed, https://doi.org/10.17190/AMF/1246109, 2016.

Miller, G. R., Chen, X., Rubin, Y., Ma, S., and Baldocchi, D. D.: Groundwater uptake by woody vegetation in a semiarid oak savanna. Water Resour. Res., 46, W10503, https://doi.org/10.1029/2009WR008902, 2010.

Miller, G. R., Baldocchi, D. D., Law, B. E., and Meyers, T.: An analysis of soil moisture dynamics using multi-year data from a network of micrometeorological observation sites. Adv. Water Res., 30, 1065–1081, https://doi.org/10.1016/j.advwatres.2006.10.002, 2007.

Milly, P. C. D., and Dunne, K. A.: On the hydrologic adjustment of climate-model projections: The potential pitfall of potential evapotranspiration. Earth Interact., 15(1), 1–14, https://doi.org/10.1175/2010EI363.1, 2011.

Milly, P. C. D., and Dunne, K. A.: Potential evapotranspiration and continental drying. Nat. Clim. Change, 6, 946–949, https://doi.org/10.1038/NCLIMATE3046, 2016.

Montandon, L. M., and Small, E. E.: The impact of soil reflectance on the quantification of the green vegetation fraction from NDVI. Remote Sens. Environ., 112(4), 1835–1845, https://doi.org/10.1016/j.rse.2007.09.007, 2008.

Monteith, J. L. : Evaporation and environment. Symposia of the Society for Experimental Biology, 19, 205–234, https://doi.org/10.1613/jair.301, 1965.

Moran, M. S., Scott, R. L., Hamerlynck, E. P., Green, K. N., Emmerich, W. E., and Holifield Collins, C. D.: Soil evaporation response to Lehmann lovegrass (Eragrostis lehmanniana) invasion in a semiarid watershed. Agr. Forest Meteorol., 149(12), 2133–2142, https://doi.org/10.1016/j.agrformet.2009.03.018, 2009.

Nearing, M. A., Kimoto, A., Nichols, M. H., and Ritchie, J. C.: Spatial patterns of soil erosion and deposition in two small, semiarid watersheds. J. Geophys. Res., 110, F04020, https://doi.org/10.1029/2005JF000290, 2005.

Noilhan, J., and Planton, S.: A simple parameterization of land surface processes for meteorological models. Mon. Weather Rev., 117, 536–549, 1989.

Oudin, L., Hervieu, F., Michel, C., Perrin, C., Andréassian, V., Anctil, F., and Loumagne, C.: Which potential evapotranspiration input for a lumped rainfall-runoff model? Part 2 - Towards a simple and efficient potential

evapotranspiration model for rainfall-runoff modeling. J. Hydrol., 303(1–4), 290–306, https://doi.org/10.1016/j.jhydrol.2004.08.026, 2005.

Paltridge, G. W.: Global dynamics and climate – A system of minimum entropy exchange. Q. J. Roy. Meteor. Soc., 101, 475–484, 1975.

Pietroniro, A., Soulis, E., Snelgrove, K., and Kouwen, N.: A framework for coupling atmospheric and hydrological models, in: Soil-Vegetation_Atmosphere Transfer Schemes and Large-Scale Hydrological Models, edited by: Dolman, A. J., Hall, A. J., Kavvas, M. L., Oki, T., and Pomeroy, J. W., IAHS publication no 270, IAHS Press, Wallingford, 27-34, 2001.

Porada P., Kleidon, A., and Schymanski, S. J.: Entropy production of soil hydrological processes and its maximisation. Earth Syst. Dynam., 2, 179–190, https://doi.org/10.5194/esd-2-179-2011, 2011.

Porporato, A., Laio, F., Ridolfi, L., and Rodriguez-Iturbe, I.: Plants in water-controlled ecosystems: active role in hydrologic processes and response to water stress III. Vegetation water stress. Adv. Water. Resour., 24, 745–762, https://doi.org/10.1016/S0309-1708(01)00007-0, 2001.

Priestley, C. H. B., and Taylor, R. J.: On the Assessment of Surface Heat Flux and Evaporation Using Large-Scale Parameters. Mon. Weather Rev., 100(2), 81–92, https://doi.org/10.1175/1520-0493(1972)100<0081:OTAOSH>2.3.CO;2, 1972.

Prudhomme, C., and Williamson, J.: Derivation of RCM-driven potential evapotranspiration for hydrological climate change impact analysis in Great Britain: A comparison of methods and associated uncertainty in future projections. Hydrol. Earth Syst. Sc., 17(4), 1365–1377, https://doi.org/10.5194/hess-17-1365-2013, 2013.

Pryor, S. C., Barthelmie, R. J., Young, D. T., Takle, E. S., Arritt, R. W., Flory, D., et al.: Wind speed trends over the contiguous United States. J. Geophys. Res.-Atmos., 114, D14105, https://doi.org/10.1029/2008JD011416, 2009.

Reichstein, M., Falge, E., Baldocchi, D., Papale, D., Aubinet, M., Berbigier, P., et al. : On the separation of net ecosystem exchange into assimilation and ecosystem respiration: Review and improved algorithm. Global Change Biol., 11, 1424–1439, https://doi.org/10.1111/j.1365-2486.2005.001002.x, 2005.

Schaefli, B., and Gupta, H. V.: Do Nash values have value? Hydrol. Process., 21, 2075–2080, https://doi.org/10.1002/hyp.6825, 2007.

Scott, R. L.: AmeriFlux US-Wkg Walnut Gulch Kendall Grassland, https://doi.org/10.17190/AMF/1246112, 2016.

Scott, R. L., Hamerlynck, E. P., Jenerette, G. D., Moran, M. S., and Barron-Gafford, G. A.: Carbon dioxide exchange in a semidesert grassland through drought-induced vegetation change. J. Geophys. Res. 115, G03026, https://doi.org/10.1029/2010JG001348, 2010.

Scott, R. L., and Biederman, J. A.: Partitioning evapotranspiration using long-term carbon dioxide and water vapor fluxes. Geophys. Res. Lett., 44(13), 6833–6840, https://doi.org/10.1002/2017GL074324, 2017.

Seiller, G., and Anctil, F.: How do potential evapotranspiration formulas influence hydrological projections? Hydrolog. Sci. J., 61(12), 2249–2266, https://doi.org/10.1080/02626667.2015.1100302, 2016.

Shannon, C.: A mathematical theory of communication. Bell System Technical Journal, 27, 379–423, https://doi.org/10.1016/S0006-3495(96)79210-X, 1948.

Shaw, S. B., and Riha, S. J.: Assessing temperature-based PET equations under a changing climate in temperate, deciduous forests. Hydrol. Process., 25(9), 1466–1478, https://doi.org/10.1002/hyp.7913, 2011.

Sheffield, J., Wood, E. F., and Roderick, M. L.: Little change in global drought over the past 60 years. Nature, 491(7424), 435–438, https://doi.org/10.1038/nature11575, 2012.

5 Shi, Y., Davis, K. J., Zhang, F., and Duffy, C. J.: Evaluation of the Parameter Sensitivities of a Coupled Land Surface Hydrologic Model at a Critical Zone Observatory. J. Hydrometeorol., 15(1), 279–299, https://doi.org/10.1175/JHM-D-12-0177.1, 2014.

Shuttleworth, W. J., and Wallace, J. S.: Evaporation from sparse crops – an energy combination theory. Q. J. Roy. Meteor. Soc., 111, 839–855, 1985.

10 Šimůnek, J., Šejna, M., Saito, H., Sakai, M., van Genuchten, M. Th.: The HYDRUS-1D software package for simulating the one-dimensional movement of water, heat, and multiple solutes in variably-saturated media, version 4.17. HYDRUS Software Series 3, Department of Environment Sciences, University of California Riverside, 2013.

Thom, A. S.: Momentum, mass, and heat exchange of plant communities, in: Vegetation and the Atmosphere, edited by Monteith, J. L., Academic Press, London, 57-109, 1975.

15 Thompson, J. R., Green, A. J., and Kingston, D. G.: Potential evapotranspiration-related uncertainty in climate change impacts on river flow: An assessment for the Mekong River basin. J. Hydrol., 510, 259–279, https://doi.org/10.1016/j.jhydrol.2013.12.010, 2014.

Thornthwaite, C. W.: An approach toward a rational classification of climate. Geogr. Rev., 38(1), 55–94, 1948.

Tuzet, A., Perrier, A., and Leuning, R.: A coupled model of stomatal conductance, photosynthesis and transpiration. Plant Cell Environ., 26, 1097–1116, https://doi.org/10.1046/j.1365-3040.2003.01035.x, 2003.

van Genuchten, M. T.: A closed-form equation for predicting hydraulic conductivity of unsaturated soils. Soil Sci. Soc. Am. J., 44, 892-898, 1980.

Verbist, K. M. J., Pierreux, S., Cornelis, W. M., McLaren, R., and Gabriels, D.: Parameterizing a coupled surface-subsurface three-dimenional soil hydrological model to evaluate the efficiency of a runoff water harvesting technique. Vadose Zone J., 11(4), vzj2011.0141, https://doi.org/10.2136/vzj2011.0141, 2012.

Verhoef, A., and Egea, G.: Modeling plant transpiration under limited soil water: Comparison of different plant and soil hydraulic parameterizations and preliminary implications for their use in land surface models. Agr. Forest Meteorol., 191, 22–32, https://doi.org/10.1016/j.agrformet.2014.02.009, 2014.

Wagener, T.: Can we model the hydrological impacts of environmental change? Hydrol. Proc., 21, 3233–3236, https://doi.org/10.1002/hyp.6873, 2007.

30

Wang, J., and Bras, R.: A model of surface heat fluxes based on the theory of maximum entropy production. Water Resour. Res., 45, W11422, https://doi.org/10.1029/2009WR007900, 2009.

Wang, J., and Bras, R.: A model of evapotranspiration based on the theory of maximum entropy production. Water Resour. Res., 47, W03521, https://doi.org/10.1029/2010WR009392, 2011.

35 Wang, Y., and Leuning, R.: A two-leaf model for canopy conductance, photosynthesis and partioning of available energy. II. Comparison with measurements. Agr. Forest Meteorol., 91, 89–11, https://doi.org/10.1016/S0168-1923(98)00061-6, 1998.

Wang, J., Bras, R., Nieves, V., and Deng, Y.: A model of energy budgets over water, snow, and ice surfaces. J. Geophys. Res.-Atmos., 119, 6034–6051, https://doi.org/10.1002/2013JD021150, 2014.

Wang, J., Bras, R., Sivandran, G., and Knox, R.: A simple method for the estimation of thermal inertia. Geophys. Res. Lett., 37, L05404, https://doi.org/10.1029/2009GL041851, 2010.

5   Wang, H., Tetzlaff, D., and Soulsby, C.: Testing the maximum entropy production approach for estimating evapotranspiration from closed canopy shrubland in a low-energy humid environment. Hydrol. Process., 31(25), 4613–4621, https://doi.org/10.1002/hyp.11363, 2017.

Westhoff, M. C., and Zehe, E.: Maximum entropy production: can it be used to constrain conceptual hydrological models? Hydrol. Earth Syst. Sc., 17, 3141–3157, https://doi.org/10.5194/hess-17-3141-2013, 2013.

10 Wilson, K. B., and Baldocchi, D. D.: Seasonal and interannual variability of energy fluxes over a broadleaved temperate deciduous forest in North America. Agr. Forest Meteorol., 100(1), 1–18, https://doi.org/10.1016/S0168-1923(99)00088-X, 2000.

Wilson, K. B., Hanson, P. J., Mulholland, P. J., Baldocchi, D. D., Wullschleger, S. D.: A comparison of methods for determining forest evapotranspiration and its components: sap-flow, soil water budget, eddy covariance and
15   catchment water balance. Agr. Forest Meteorol., 106, 153–168, 2001.

Xu, C., and Singh, V. P.: Evaluation and generalization of temperature-based methods for calculating evaporation. Hydrol. Process., 15, 305–319, 2001.

Xu D, Agee E, Wang J, Ivanov VY. Estimation of Evapotranspiration of Amazon Rainforest Using the Maximum Entropy Production Method. Geophys. Res. Lett 46 (3): 1402–1412 DOI: 10.1029/2018GL080907, 2019.

20 Zabel, F., and Mauser, W.: 2-way coupling the hydrological land surface model PROMET with the regional climate model MM5. Hydrol. Earth Syst. Sc., 17, 1705–1714, https://doi.org/10.5194/hess-17-1705-2013, 2013.